Targeting Borrelia burgdorferi's Heat Shock Protein for the Diagnosis and Treatment of Lyme Disease

by

Madeline Graham Sell

Department of Pharmacology and Cancer Biology
Duke University

Date:_____

Approved:

_____
Cynthia Kuhn, Supervisor

_____
David MacAlpine

_____
James Alvarez

_____
Emily Derbyshire

Dissertation submitted in partial fulfillment of
the requirements for the degree of Doctor
of Philosophy in the Department of
Pharmacology and Cancer Biology in the Graduate School
of Duke University

2020

ABSTRACT

Targeting Borrelia burgdorferi's Heat Shock Protein for the Diagnosis and Treatment of Lyme Disease

by

Madeline Graham Sell

Department of Pharmacology and Cancer Biology
Duke University

Date:_____

Approved:

_____
Cynthia Kuhn, Supervisor

_____
David MacAlpine

_____
James Alvarez

_____
Emily Derbyshire

An abstract of a dissertation submitted in partial
fulfillment of the requirements for the degree
of Doctor of Philosophy in the Department of
Pharmacology and Cancer Biology
in the Graduate School of
Duke University

2020

Abstract

Infections are most commonly identified by microscopy, culturing the organism, or testing the patients' blood for antigens or antibodies. These methods are unreliable in bacteria that persist in a non-dividing, metabolically inactive dormant state, leading to treatment delays and an increased risk of developing chronic morbidities. Borrelia burgdorferi (*B. burgdorferi*), the causative spirochete in Lyme Borreliosis, is an example of a stealth pathogen difficult to culture from blood, capable of evading the host immune system, and under adverse growth conditions in host tissue, able to survive in a dormant state. Despite early diagnosis and treatment, 20-35% of patients with Lyme Borreliosis experience chronic symptoms, the etiology of which remains unknown due to the lack of accurate diagnostics to demonstrate the presence of a persistent infection. In vivo diagnostic imaging of bacterial infections is currently reliant on targeting their metabolic pathways, an ineffective method to identify microbial species with low metabolic activity. Here we characterize HS-198 as a small molecule-fluorescent conjugate that selectively targets the highly conserved bacterial protein, HtpG (High temperature protein G) within *B. burgdorferi*, the bacteria responsible for Lyme Disease. We describe the use of HS-198 to target morphologic forms of B. burgdorferi in both the logarithmic growth phase and the metabolically dormant stationary phase. Furthermore, in a murine infection model, systemically injected HS-198 identified *B. burgdorferi* as revealed by imaging in post necropsy tissue sections. These findings demonstrate how small molecule probes directed at conserved

bacterial protein targets can function to identify the microbe using non-invasive imaging and potentially as scaffolds to deliver antimicrobial agents to the pathogen, potentially solving both the problem of diagnosis and treatment.

Dedication

"They are not smarter than you, they simply know more"

-Miriam Sell

Thank you for putting me on the quest to never stop learning.

Contents

List of Tables

List of Figures

Acknowledgements

I would like to thank my family first and foremost. To my late grandparents Charles Sell M.D., Sarah Sell M.D., Norman Latker JD., and Carole Latker PhD., for giving my parents and therefore myself the many opportunities that brought me to this point. I am lucky to have a family that holds education, research, and science in such high regard. Thank you to my late father, Clive Sell M.D., for setting high expectations and inspiring us to reach for the stars. Thank you to my mother Miriam Sell M.D. for being my life long best friend and biggest advocate. Thank you to my eldest brother, Benjamin Sell P.A.-c for showing me that no matter the hurdle, nothing can beat relentless hard work if you put your heart into it. Thank you to my brother David Sell PhD., the king of the nerds, for showing me that knowledge is the key. Thank you to my childhood best friends Catherine Zabilski and Sarah Stevens for always supporting me and telling everyone they knew I was the foremost expert on Lyme Disease. Thank you to Jessica Shannon, Rylee Hackley, and Emma Dolan for showing me what real life women supporting women looks like. Thank you to David Alcorta PhD. for encouraging my growth as a scientist, and Andrew Padilla and Dakota Nollner for their assistance collecting data for this project. And thank you to my late thesis advisor, Neil Spector M.D., who passed away before he could see me defend. Aside from being a wonderful mentor, he was one of the greatest advocates for Lyme Disease patients. He will be greatly missed.

1. Introduction: Lyme Disease & Diagnostic Limitations

1.1 Lyme Disease

Lyme disease is an infection of spirochete bacteria transmitted through the bite of tick. The causative strain of bacteria differs depending on location, but in the United States, Lyme Disease is caused by *Borrelia burgdorferi.* With an estimated prevalence of 340,000 new cases diagnosed every year in the United States, Lyme Borreliosis is the most common vector-borne illness in the U.S and Europe [1] [2]. This threat is only growing as the counties in the U.S. identified as high risk have increased diagnosed cases by over 300% since the 1990's [3].

Not all ticks are carriers of Lyme Disease. *Ixodes scapularis* and *Ixodes pacificus* ticks are the primary transmitters of Borrelia in the United States, but specific carriers vary in other countries [4]. Tick eggs are laid by female adults around late May and then hatch into larvae around August. These larvae then feed on an initial host, usually a small animal such as the white-footed mouse (*Peromyscus leucopus*), and then remain dormant throughout the winter. Around April the larvae molt into nymphs and feed once again. Nymphs are usually responsible for transmission of infection, which is why the summer months are most often considered high-risk "tick-season". The increase in outdoor human activity, paired with the small size of the nymph compared to adult ticks, make them more likely to remain unnoticed while attached. Finally, around September nymphs molt into adult ticks which prefer feeding on larger animals such as the white-tailed deer (*Odocoileus virginianus*) and where it will often lay its eggs. Small

animals such as the white-footed mouse act as reservoirs for Borrelia and each feeding offers a chance to infect the tick [5] [6]. Environmental changes such as rising temperatures are elongating the "tick season" and increasing their geographical distribution [7]. Additionally, deforestation and "forest defragmentation" are increasing humans interactions with animals that could be carriers for an infected tick [8].

Borrelia are not passed to the host immediately, however the exact time transmission occurs is not clear. The CDC advises that the tick must remain attached for 24- 48 hours for transmission to occur, conversely, animal studies have found transmission with ticks attached for less than 16 hours [9] [10]. While it sounds unlikely that a tick would go undetected for that length of time, the saliva of ticks contain bradykininases and amine (histamine)-binding lipocalins that breakdown histamine and bradykinins, mediators of pain and itch that would normally alert you to the presence of an insect [11, 12]. After spending time in a tick prevalent area, a visual or tactile check of your skin for quick tick removal is the best first line protection [13]. On average, 7 days post infection from a tick bite, 70-80% of people will present with an erythema mygrans (EM) rash, commonly referred to as the "bullseye" [14, 15]. "This circular or elliptic red area spreads centrifugally, reflecting movement of spirochetes through lymphatics of the skin. Subsequent central clearing gives the appearance of a "target"" [16]. Along with this rash many patients experience flu-like symptoms including fever, headache, and joint pain.

Current treatment for Lyme Disease is a single course of antibiotics, (doxycycline, ceftriaxone, or amoxicillin) and patients diagnosed and treated early often make a full recovery. However, about ten percent of patients suffer from Post-Treatment Lyme Disease Syndrome (PTLDS) and continue to express symptoms after antibiotic treatment [17]. These symptoms can be as significant as facial palsy, cardiac inflammation, and most commonly, severe rheumatoid arthritis (RA). PTLDS is not responsive to traditional therapies, and there are currently no alternative strategies. Furthermore, due to the variable symptoms, insensitive testing, and lack of disease awareness many patients will not be properly diagnosed early on. If the infection goes untreated the infection becomes systemic. Borrelia tends to infiltrate connective tissue and patients can develop Bell's palsy facial paralysis, Lyme carditis, and Lyme neuroborreliosis [18]. Recently, Borrelia has been linked to a possible initiator of Alzheimers Disease [19].

1.2 History of Lyme Vaccine

In an attempt to prevent the transmission of Lyme, in 1998 SmithKline Beecham received FDA approval for a vaccine called LYMErix. This vaccine was a recombinant *B. burgdorferi* protein of outer-surface protein A (OspA). OspA is found in high levels in the tick midgut and then downregulated at the time of spirochete migration to the host[20]. This vaccine proved safe in animals and demonstrated an efficacy of 76%. Three doses were required over a year. This vaccine was predominantly effective against *Borrelia*

burgdorferi and not all Lyme Disease strains. Ludwig & Bailey filed a class action lawsuit against the LYMErix™ SmithKlineBeecham. Investigators found:

> "In patients with the DR4+ genotype, an immune response against OspA could translate into a cross-reactive autoimmune response. By implication, an OspA Lyme vaccine might result in autoimmunity in these genetically predisposed individuals[21]".

While the FDA decided there was no need to remove this product, it did request further testing. In 2002 GlaxoSmithKline withdrew LYMErix™ from the market citing poor market performance. In the late '90's, another vaccine was produced by Pasteur Mérieux Connaught as a nonadjuvanted vaccine (ImuLyme) to the same OspA protein. Efficacy was measured at 68% after 2 doses and at 92% after 3 doses. While no specific adverse events were cited they decided not to pursue FDA approval. Reportedly, they were concerned of patent controversies with GlaxoSmithKline and a small market size for the product [22]. Today, Valneva and Pfizer are collaborating on a vaccine that is currently in Phase II of clinical trials. This vaccine is a protein subunit vaccine, once again for OspA [23].

Vaccine for animals also focus on OspA, but recent advances for veterinarian patients focus on the combination of OspA and OspC. Vangaurd, for example, contains recombinant proteins for both OspA, which they say would help kill the Borrelia inside the tick while it is attached, and OspC which can help kill the Borrelia that has successfully migrated to the animal. This vaccine is USDA approved for 15-months of immunity, which is important as OspA immunity alone is known to wane quickly [24].

As evidenced by the efficacy of LYMErix™ and ImuLyme, those that are vaccinated could still be susceptible to Lyme Disease, and the promise of a new vaccine does not diminish the need for the development of improved treatment regiments and diagnostics for active disease.

1.3 Early vs Late Detection and Treatment

A missed or delayed diagnosis of Lyme Borreliosis increases the risk of long-term morbidity related to chronic arthritis, neuropsychiatric symptoms, Lyme carditis, and other debilitating conditions [25]. "*B. burgdorferi* can switch from motile cellular forms into several defensive morphological forms such as round bodies, stationary phase, persister cells, and biofilm" [26]. Biofilms are adherent microbial communities; they consist of aggregates encapsulated in an extracellular polymeric matrix(EPS) that often contain extracellular DNA, heat shock proteins, and other secreted proteins [27]. Early stage Borrelia which exist predominantly in a classic spirochete morphology are highly susceptible to common antibiotic treatment [13]. Borrelia in later stages of culturing show an increase in stationary phase morphologies that include persister cells and biofilm formation [28]. In vitro studies under clinically non-relevant conditions suggest that round bodies and stationary phase Borrelia might be able to revert to spirochetes only if exposed to the unfavorable conditions < 4 hours. The clinical relevance remains unproven [28].

Recently, evidence of biofilm development by *B. burgdorferi* has been discovered in untreated Lyme disease patients [29]. Furthermore, biofilms have been found to

induce a more severe inflammatory response and are linked to persistence and antibiotic resistance [30] [31] [32]. Additionally, persister cells show a decrease in ATP production pointing to a dormant state which also makes them less susceptible to antibiotic treatment [28, 33]. Evidence from studies in animal models of Lyme Borreliosis and in infected humans points to active infection with *B. burgdorferi* as a probable underlying cause of the chronic symptoms in some individuals [34-37]. It has been reported that as many as 36% of individuals with Lyme Borreliosis will experience persistent symptoms [38]. This increased risk for delayed diagnosis points to a need for improved diagnostic approaches.

1.4 Difficulties Detecting B. burgdorferi

> Currently, no single diagnostic method is uniformly accurate in the assessment of early Lyme disease; most new techniques are not widely available and conventional serology has a low sensitivity. Clinical assessment by experienced healthcare personnel remains the most accurate method in endemic areas[5].

Direct diagnosis of bacterial infections has historically relied on culturing microbes from blood or other body fluids and tissues. However, isolation of fastidious bacterial microbes, especially those that rapidly disseminate from circulation into tissues, including *Borrelia burgdorferi*, represent a diagnostic challenge [39]. The CDC recommends a two-tiered test. First, an enzyme immunoassay (EIA) or immunofluorescence assay (IFA) [40]. If that test is positive then an IgG and IgM western blot should also be performed. All of these tests are serologic immunoassays designed to detect antibodies formed as part of the hosts immune response. Stealth

organisms, including Borrelia, have mechanisms to evade the host response, making these tests insensitive and inaccurate especially in the setting of late stages of infection [41]. The average sensitivity, or 'probability a positive sample will be defined as positive by the test', of the common diagnostic method of Western blots is only 62.4% and ELISA is 62.3% [2]. In addition, progression of the disease and the treatment itself can blunt the antibody immune response making follow up testing not informative [42].

> "The initially significant immune system activation was followed by a loss of the specific humoral immune response and a decrease in the cellular immune response to B. burgdorferi over the course of the disease. Viable spirochetes were identified" [43].

There is a need for more sensitive testing as well as testing capable of being utilized post treatment to verify the infection has been eradicated.

One strategy to overcome the challenge of diagnosing stealth organisms, like *B. burgdorferi,* which exit the circulation soon after initial infection, is the development of imaging probes. There is currently no method for using imaging to diagnose Lyme disease. Direct detection of the pathogen confirms infection, and for this reason many researchers are seeking to develop imaging probes to visualize infection *in vivo*. These probes would allow whole body visualization and unlike select tissue samples they would provide the ability to monitor disease during and after treatment. Imaging *B. burgdorferi in vivo* intermittently through the duration of treatment may provide an objective and quantitative indicator of clinical response, and therefore guide the duration of therapy.

To date, imaging strategies have largely targeted metabolic pathways utilized by bacteria, including the maltodextrin transporter expressed in gram-negative and positive-bacteria and 2-[^{18}F]-fluorodeoxysorbitol that utilizes sorbitol, a metabolic substrate for *Enterobacteriaceae* [44] [45]. In addition, fluorine 18-fluorodeoxyglucose (^{18}F -FDG) positron emission tomography (PET) has been used to identify foci of increased glucose uptake, including inflammation, infection and malignancies [46]. Although targeting metabolic pathways may be effective in actively replicating bacteria with high metabolic requirements, persister and stationary growth phase bacteria exhibit low metabolic activity and are therefore not amenable to this approach [47]. Importantly, none of these imaging approaches are capable of Lyme diagnostics.

Efforts to develop more sensitive Borrelia testing have been hindered to date by the lack of a probe that can specifically target a *Borrelia* protein that is highly abundant in all clinically relevant morphological states. Antigenic variation, the process by which the sequence of an expressed protein changes over time, as well as the change in expression of outer surface proteins during *B. burgdorferi's* life cycle, are two mechanisms that hinder the development of precise diagnostics [48]. Tests preferentially targeting these outer surface proteins, the most abundant proteins, are only targeting specific stages of its life cycle. Furthermore, plasmid variation between strains, and large genetic variation between species make developing a Borrelia specific test difficult.

1.5 Bacterial HtpG

High temperature protein G (HtpG), the prokaryotic homologue of the 90 kDa mammalian heat shock protein (Hsp90), is an attractive target for diagnostic and potential therapeutic interventions for Lyme Borreliosis. HtpG is a highly expressed molecular chaperone found in most bacterial species [49]. We hypothesized it could be useful in detecting the presence of *B. burgdorferi* which is known for antigenic variation, loss of plasmids, and change in outer surface protein expression that hinders the ability to identify diagnostic protein targets[48]. Encoded on the linear chromosome of *Borrelia* rather than a plasmid, HtpG is conserved across different pathogenic species and strains of *B. burgdorferi* (Figure 1) and is expressed throughout the different growth phases of *Borrelia*, which is essential when developing a targeted imaging probe [50].

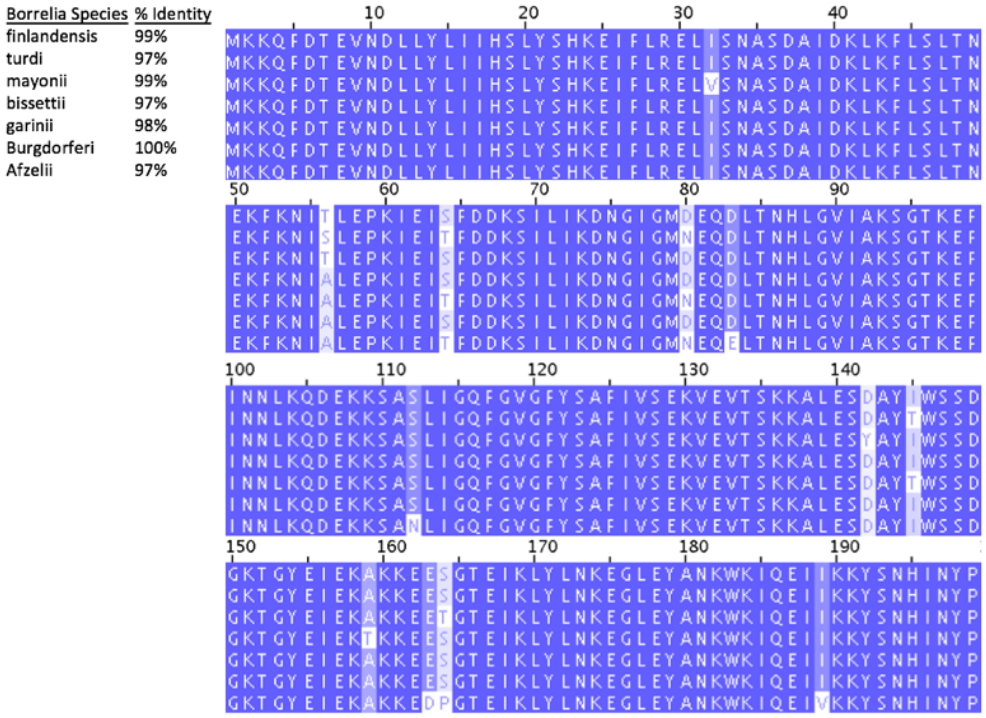

Figure 1: Sequence alignment of HtpG from Borrelia spirochete utilizing Clustal Omega Multiple Sequence Alignment Program

Although less is known about the function of *Borrelia* HtpG, the eukaryotic homologue, Hsp90, is involved in maintaining intracellular proteostasis by regulating protein folding, trafficking, and preventing aggregation of denatured proteins [49, 51]. Bacterial HtpG deletion and mutation is not lethal in most bacteria, based on information gathered in *E. coli*, *Actinobacillus actinomycetemcomitas*, and *Bacillus subtilis*. *Saccharomyces cerevisiae* is one of few prokaryotes that demonstrate lethality. Serum from confirmed Lyme disease patients contains HtpG antigen and antibodies specific to HtpG, indicating immunogenicity of the protein [52]. HtpG-dependent infection persistence has been characterized in several prokaryotic species. HtpG was found to induce an inflammatory cascade via IL-8 in *P. gingivalis*. In *P. aeruginosa* and *E.*

coli null mutants were found to have impaired biofilm formation, reduced virulence, and reduced resistance to antibiotics. HtpG was nonessential for establishing infection by *Salmonella typhimurium,* but was required to sustain its infection over time [54]. HtpG expression positively correlates with biofilm formation and pathogenicity in *P. intermedia.* HtpG was found to be actively secreted as a virulence factor in *A. salmonicida* [53-56]. Therefore, HtpG from multiple pathogenic prokaryotic species has been implicated in development of biofilm, antibiotic resistance, and inflammatory responses in the host. While inhibiting HtpG might not kill most prokaryotes, HtpG's abundance, consistent expression, and role in biofilms make HtpG a drug target of choice for delivering payloads. Ligands selective for HtpG may be linked to compounds effective in killing latent Borrelia, which are not normally susceptible to typical antibody treatments.

Amino acid sequence alignment from different prokaryotes and eukaryotic Hsp90, demonstrates high conservation around the ATP binding regions (Figure 2). Identical amino acids across all species are highlighted in dark blue and those with decreasing % of identity shown in correspondingly lighter shades.

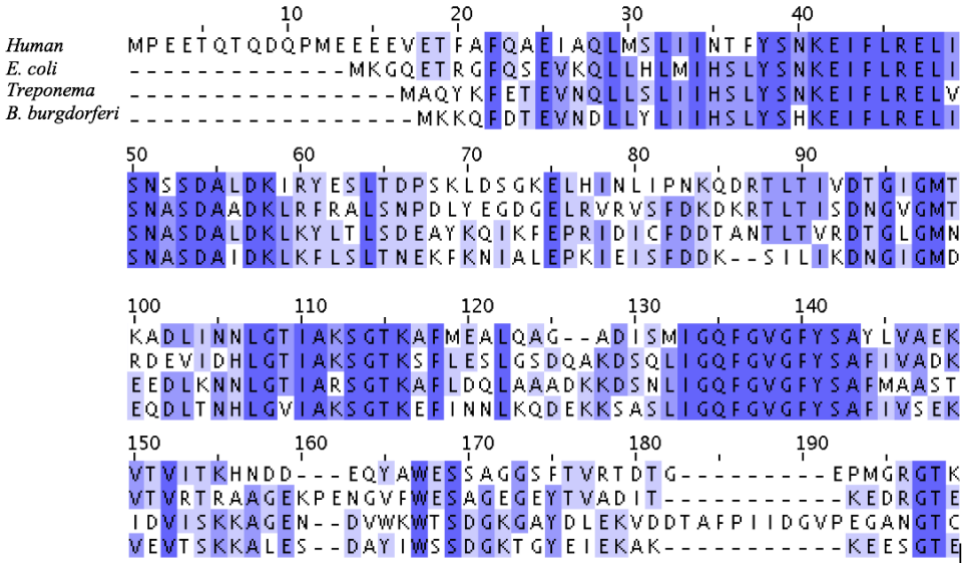

Figure 2: Protein sequence alignment of ATPase domains of Human Hsp90, E. coli HtpG, T. denticola HtpG, and B. burgdorferi HtpG. Identical amino acids across all species are highlighted in dark blue and those with decreasing % of identity shown in correspondingly lighter shades.

However, the intervening amino acids between the conserved residues are often quite different, even across closely related prokaryotic forms. In order to minimize host toxicity, as well as to increase confidence in the ability to diagnose infection, these drugs need to be highly selective for the HtpG expressed in the intended targeted pathogen. While the majority of research into Hsp90 has been in regards to non-specific high potent molecules, recent work in pathogenic fungus, *Candida*, and *Leishmania* demonstrates that the differences between conserved residues may be exploited to create species selective agents [57] [58] [59]. We therefore reasoned that these differences may be sufficient to design small molecules that can similarly discriminate HtpG of stealth organisms, leading to a delivery agent specific for *B. burgdorferi* and serve as a model for selectively delivering payloads to other pathogens. This payload could include imaging

agents or potent toxins for treatment. The purpose of this work was to identify a small molecule ligand able to selectively bind HtpG and tether to a payload of interest.

2. Experimental Methods

2.1 GFP-fusion Protein Plasmid Construction

The *B. burgdorferi, E.coli, and Treponema denticoli* HtpG DNA sequences were PCR cloned from genomic DNAs using primers designed to allow in-frame ligation independent cloning with GFP in the IPTG inducible bacterial expression vector, 1GFP (pET His6 GFP TEV LIC cloning vector (1GFP) was a gift from Scott Gradia (Addgene plasmid # 29663)). Human Hsp90-alpha was similarly cloned from cDNA generated from the human breast epithelial line, Mcf10A. Fusion protein cloning was done using the ligation independent cloning procedure via single nucleotide T4 DNA polymerase treatment of vector and purified PCR products then annealing of complementary single strand ends before transformation into DH5 *E. coli*. Proper fusion junctions and fidelity of HSP inserts were confirmed by sequencing, then the plasmid was transformed into *E. coli* BL21(DE3) for protein expression. Fusion protein synthesis was induced by incubation with 1 mM IPTG or autoinduction [36]. Production of GFP-HtpG/Hsp90 was confirmed by identification of GFP and HtpG peptides with MALDI using an ABSciex 5800 TOF/TOF mass spectrometer in the induced band identified on a SDS-PAGE gel. Several liters of induced cultures were generated, pelleted with centrifugation, flash frozen in liquid nitrogen and then stored at -80 ^{o}C until subsequent FLECS analysis.

2.2 Fluorescent Linked Enzyme Chemoproteomic Strategy (FLECS) Assay

γ-Linked ATP Sepharose matrix was generated as described previously by the Haystead lab [19]. BL21 bacterial pellets expressing GFP-fusion proteins of *E. coli, B. burgorferia, T. denticola* HtpGs and human Hsp90 were lysed with B-PER Complete Bacterial Protein Extraction Reagent (ThermoScientific 89821) and centrifuged at 35,000 rpm (Beckman coulter type 45 Ti Fixed Angle Rotor) to pellet remaining BL21 material. The clarified lysate was added to a column containing ATP bound sepharose. The column was washed with low salt buffer [150 mM NaCl, 25 mM of HEPES, pH 7.4, 1 mM of DTT, and 60 mM MgCl2], followed by high salt buffer [1M NaCl, 25 mM of HEPES, pH 7.4, 1 mM of DTT, 0.1% IGEPAL, and 60 mM MgCl2] and once again low salt buffer to remove unbound protein. Next, the resin with bound proteins (50 μl) was transferred to 0.2 μm polyvinylidene fluoride filter 96-well plate (Corning) sitting on top of a black flat-bottomed 96-well catch plate (Corning). Small molecules or ATP were added to each well (50 μl) and the plates were centrifuged using an Eppendorf Centrifuge 5810 at 1,100 rpm for 1 min. The eluted proteins were measured in a fluorescent plate reader to detect the GFP. As a means to confirm the presence of HtpG verses fluorescent compounds that could cause an assay signal, samples were analyzed by SDS-PAGE followed by silver stain and mass spectrometry.

2.3 B. burgdorferi Bacterial Growth

B. burgdorferi strain B31 was obtained from ATCC (ATCC 35210). Cultures were grown in Barbour–Stoenner–Kelly medium (BSK-II) without gelatin [16] and supplemented with 6% rabbit serum at 34 °C. Low passage cultures (less than 4) were utilized. Later stage morphological variants were obtained by increasing culture time to approximately 8 days to achieve a density of ~10^8.

2.4 B. burgdorferi Bacterial Imaging

Bacterial cultures in logarithmic or stationary phase were incubated in media for 1 hour with 10 μM HS-198 and wheat germ agglutinin (WGA) conjugated with Alexa 488 at 10 μg per ml (Biotium Cat #29022), cells were then washed with fresh media and mounted onto the slide with prolong Gold mounting solution containing DAPI. Samples were visualized using a Zeiss Axio Imager Upright microscope, 62X oil objective, 405, 488 or 633 nm laser and DIC.

2.5 Immunohistochemistry

10μm sections of frozen tissues were incubated with WGA (Biotium Cat #29077) for 1 hour in PBS. Tissues were washed and fixed with 3:1 methanol to acetic acid. Slides were incubated with FITC conjugated *B. burgdorferi* polyclonal antibody (Thermo Fisher Cat # PA173005) for 1 hour at room temperature. Non-injected or infected tissues were washed and incubated with 1 μM of HS-198 for 30 minutes as control, injected tissues were not incubated with HS-198. Slides were washed and mounted with DAPI prolong

Gold. Imaged using a Zeiss Axio Imager Upright microscope, 62X oil objective, 405, 488 or 633nm laser and DIC. Images were analyzed using FIJI software.

2.6 Correlative Light Electron Microscopy

CLEM (Correlative Light Electron Microscopy) was performed by Shannon Modla and Jeff Caplan at the bioimaging center of the Delaware Biotechnology Institute. Cells were attached to an Ibidi μ-dish containing an imprinted 500 μm cell location grid using 4% PFA for 20 min. Cells were then incubated with 10μM of HS-198 for 10 minutes followed by PBS. Cells were given to the Delaware institute for further processing and imaged using Zeiss 880 Airyscan. The alphanumeric pattern from the Ibidi μ-dish was imprinted on the freshly exposed surface of the resin, which allowed the same region of interest imaged by light microscopy to be reidentified in the ultramicrotome. Ultrathin serial sections were collected using a Leica UC7 ultramicrotome and picked up onto 2 x 1 copper slot grids, which were then dried on a domino rack (Electron Microscopy Sciences; Cat No 70621) coated with 0.5% formvar in ethylene dichloride. Serial sections were examined on a Libra 120 transmission electron microscope operating at 120kV, and images were acquired with a Gatan Ultrascan 1000 CCD using Gatan Digital Micrograph software. To capture TEM images of the entire bacterium, overlapping images were collected at 5000X and 16000X magnifications and then stitched together using the ImageJ plug-in MosaicJ.

2.7 Animals, spirochetal inoculation, and treatment

Practices in the housing and care of mice conformed to the regulations and standards of the Public Health Service Policy on Humane Care and Use of Laboratory Animals, and the Guide for the Care and Use of Laboratory Animals. The Tulane National Primate Research Center (TNPRC) is fully accredited by the Association for the Assessment and Accreditation of Laboratory Animal Care-International. The Tulane University Institutional Animal Care and Use Committee approved all animal-related protocols, including the infection and sample collection from mice.

In vivo mouse model for tissue studies: Seven C3H/HeN (Charles River labs) mice were anesthetized with isoflurane gas, 1.5-2%. Mice were infected with 500,000 logarithmic stage *B. burgdorferi* strain N40 in < 0.5 ml sterile saline by subcutaneous injection in the nape of the neck via 25-gauge needle. Ear punch biopsies were collected from mice at 7 and14 days post-inoculation to confirm infection. Disposable 2mm punches were used on the outer rim of the ear to collect skin from anesthetized mice. The biopsies were placed in BSK-H (Sigma) culture medium and grown for 2 weeks to confirm infection. After 3 weeks, mice were injected with 25nmol/animal of HS-198 in the tail vein with a tuberculin needle. 6 hours later mice were euthanized by CO2 inhalation, followed by harvest and flash-freezing of tissues, including the ear skin, spleen and tibiotarsal joints.

3. Identifying an HtpG Selective/Specific Compound

Multiple sequence alignment of the N-terminal ATP domains of *B. burgdorferi* HtpG, *E. coli* HtpG, *Treponema denticola* HtpG, and Human Hsp90 shows significant overall homology, particularly at regions that make direct contact with ATP (Fig 2) [60]. Subtle single amino acid differences are present within the catalytic clefts of these proteins, especially between residues that contact the nucleotide. We reasoned that these differences may be sufficient to design small molecules that can similarly discriminate HtpG of stealth organisms. To test this hypothesis, we utilized a Fluorescent Linked Enzyme Chemoproteomic Strategy (FLECS) assay to test known Hsp90 inhibitors for binding to various HtpG constructs [61]. First, we cloned and expressed in *E. coli* recombinant N-terminal GFP fusion forms of HtpG from *B. burgdorferi, E.coli* and *Treponema denicola,* the oral spirochete, as well as human Hsp90. We then incubated lysate after protein expression with an ATP sepharose resin to enable binding. In this assay, ATP is tethered to sepharose beads via its γ-phosphate enabling the nucleotide to bind to ATP-binding proteins such as Hsp90 and HtpG, but is non-hydrolyzable [62]. After proteins are bound to the ATP sepharose resin, small molecules with affinity to the ATP-binding site will cause elution, which can readily be detected and quantified via the GFP reporter. Elutions were confirmed through an SDS-PAGE gel and further using MALDI mass spectrometry.

We measured protein elution as a function of drug concentration for PU-H71, Ganetespib, Radicicol, Geldanamycin, HS-198, HS-131, and HS-10 (Figure 3). The ATP affinity curves were utilized to identify the IC_{50} and then find the relative K_m of each species as compared to published Human Hsp90 value (K_m=300 μM) (Table 1). The K_m of each species was then used to calculate the K_d's as shown in Table 2.

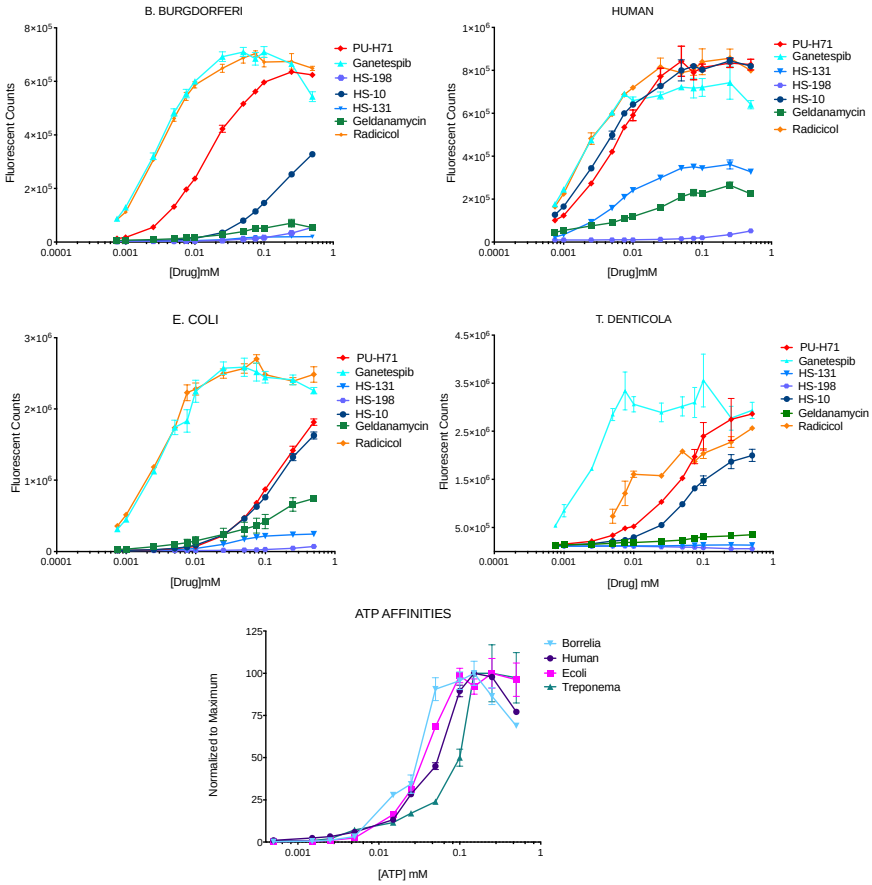

Figure 3: GFP-bound Hsp90 homologues eluted with the Hsp90 inhibitors (n=3). PU-H71, Ganetespib, Geldenamycin, Radicicol, HS-198, HS-131, and their ligand without the fluor, HS-10, eluted Hsp90 homologues from ATP-sepharose beads in the FLECS assay. The ATP affinity curves were utilized to identify the IC_{50} and then find the relative K_m of each species as compared to published Human Hsp90 value (K_m=300 μM) (Table 1). The K_m of each species was then used to calculate the K_d's as shown in Table 1.

These compounds were selected for testing based on their known binding to Human Hsp90 [63, 64]. To calculate the apparent dissociation constant ($K_{d\ app}$) for each compound, we first calculated the Michaelis Constant ($\boldsymbol{K_m}$) of *B. burgdorferi, E. coli, and T. denticola* HtpG for ATP (Fig 3) relative to the published human value ($\boldsymbol{K_m} = \mathbf{300}\ \boldsymbol{\mu M}$), $\frac{K_m(new\ species)}{K_m\ (published\ human)} = \frac{EC_{50}(new\ species)}{EC_{50}(human)}$, to be 170 $\boldsymbol{\mu}M$ M, 220 $\boldsymbol{\mu}M$ M, and 510 $\boldsymbol{\mu}M$ respectively [65]. Previously published results for *E. coli* ($\boldsymbol{K_m}$ of 250±82 $\boldsymbol{\mu}$M) are consistent with this method of analysis [66].

Table 1: Km of ATP for HtpG and Hsp90

E. coli *(μM)*	***B. burgdorferi(μM)***	***Human (μM)***	***T. denticola (μM)***
220	170	300	510

$\boldsymbol{K_d's}$ of all drugs tested in Fig 3 were calculated using $\boldsymbol{K_d = EC_{50}/1+[Resin\ ligand/K_m]}$ and shown in Table 2. Several known Human Hsp90 inhibitors also bound to the three bacterial HtpGs, demonstrating they lack species selectivity.

Table 2: K_D′s of known Hsp90 inhibitors

	E. coli (μM)	*B. burg (μM)*	*Human (μM)*	*T. dent (μM)*
HS-198	5.8 +/- 0.6	5.6 +/- 3	---	---
HS-131	1.3	1 +/- 0.1	0.3	---
HS-10	4.1 +/-1	3.5+/-0.3	0.2	7+/- 4
Radicicol	0.1	0.1	0.09	3.0 +/- 2
PU-H71	4.3 +/- 1	0.5	0.3	5 +/- 3
Ganetespib	0.1	0.1	0.1	0.03
Geldanamycin	2.5 +/- 0.4	1.2 +/- 0.2	0.9	5 +/- 3

The fluor-tethered Hsp90 inhibitor HS-131, the non-tethered ligand analog (HS-10), and the inactive fluor-tethered analog N, N-dimethylamide (HS-198) were also investigated binding to the recombinant proteins (Figure 4). Structures of HtpG inhibitors HS-198 and HS-131 are defined (Figure 4A). Fluorescent counts of drug induced GFP-bound B. burgdorferi HtpG elution characterized (Figure 4B). Fluorescent counts of drug induced GFP-bound Human Hsp90 elution characterized (Figure 4C). Fold change in HS-198 eluted fluorescent counts in *B. burgdorferi* HtpG, *E. coli* HtpG, human Hsp90 and *T. denticola* HtpG normalized to baseline (Figure 4D). Fold change in HS-131 eluted fluorescent counts in *B. burgdorferi* HtpG, *E. coli* HtpG, human Hsp90 and *T. denticola* HtpG normalized to baseline (Figure 4E).

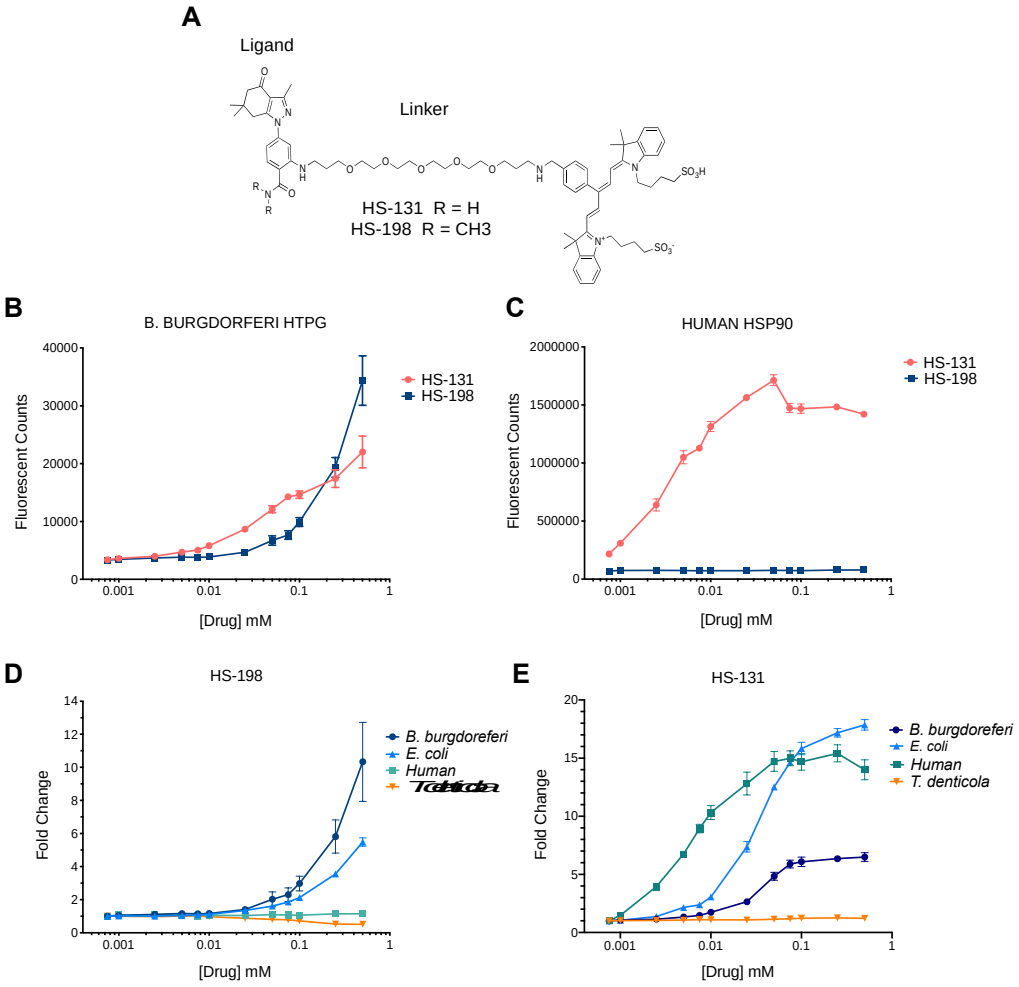

Figure 4: Structures and elution profiles of GFP-bound Hsp90 homologues with Hsp90 inhibitors (n=3). (A) Structures of HtpG inhibitors HS-198 and HS-131. (B) Fluorescent counts of drug induced GFP-bound *B. burgdorferi* HtpG elution. (C) Fluorescent counts of drug induced GFP-bound Human Hsp90 elution. (D) Fold change in HS-198 eluted fluorescent counts in *B. burgdorferi* HtpG, *E. coli* HtpG, human Hsp90 and *T. denticola* HtpG normalized to baseline. (E) Fold change in HS-131 eluted fluorescent counts in *B. burgdorferi* HtpG, *E. coli* HtpG, human Hsp90 and *T. denticola* HtpG normalized to baseline.

In prior studies, HS-131 was found to localize to Hsp90 allowing for selective discrimination of human tumor cells exhibiting a malignant phenotype from non-

transformed human epithelial cells [64]. HS-198 was designed as an inactive analog to HS-131 as the addition of methyl groups in place of hydrogens on the ligand prevented the molecule from binding to mammalian Hsp90 [64]. When the FLECS assay was performed with *B. burgdorferi* GFP-HtpG, both HS-131 and HS-198 selectively eluted the bound fusion protein from the ATP sepharose beads (Fig 4B). As expected from prior work, HS-131 effectively released recombinant human GFP-Hsp90 from the ATP sepharose beads while HS-198 did not (Fig 4C). HS-198 was the only inhibitor to target bacterial HtpG over Hsp90 (Figure 4 and Table 1). The method for calculating the K_d's were confirmed by comparison to the published results of Ganetespib [67]. HS-198 was unable to release *T. denticola* HtpG from the immobilized ATP resin, similar to human Hsp90. *E. coli* HtpG was released by HS-198 but exhibited minimally lower affinity than *B. burgdorferi* (Fig 4D). The selectivity of HS-131 was also found to show considerable variation across species (Fig 4E). In particular this molecule was completely inactive against *T. denticola* HtpG (Fig 4D). The finding that *T. denticola* is not recognized by HS-131 or HS-198 suggests that the latter probe can be used to diagnose the presence of *B. burgdorferi* over the related oral spirochete while not interacting with mammalian Hsp90.

4. HS-198 Selectively Targeting HtpG

4.1 Immunohistochemistry

Due to HS-198's ability to bind *B. burgdorferi* HtpG, but not mammalian Hsp90, we investigated the selectivity of the fluorescent probe against live cultures of *B. burgdorferi*. HS-198 at 10 μM accumulates in *B. burgdorferi* in all of its morphological states including spirochetal, blebs, and aggregates (Fig 5) as evidence by colocalization with DAPI. HS-198 was found to discretely bind the extra polymeric substance exported by *B. burgdorferi* as demonstrated by co-staining with Wheat Germ Agglutinin (WGA), a lectin that binds to N-acetyl-D-glucosamine, commonly used to identify extracellular matrices (Figure 5). When incubated for 1 hour with 10 μM of HS-198, we routinely observed HS-198 uptake in >90% of *B. burgdorferi* spirochetes.

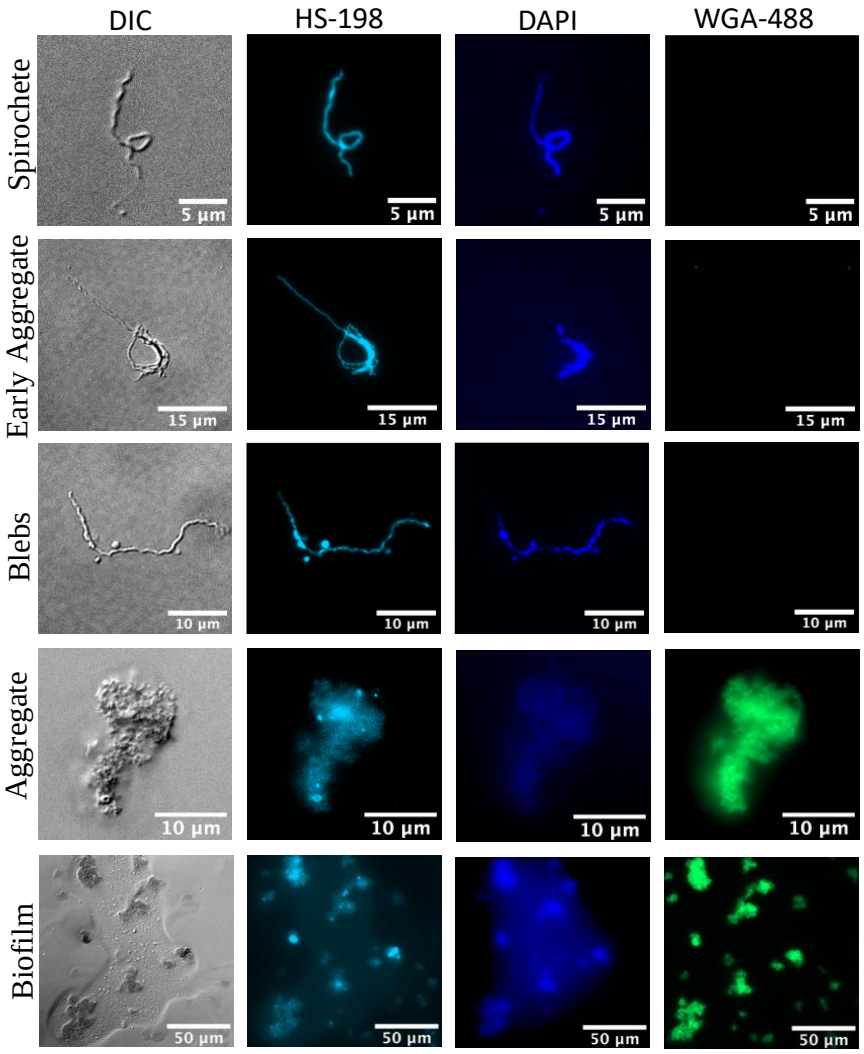

Figure 5:Fluorescent imaging of B. burgdorferi in varying morphologies incubated with HS-198, WGA-488, and DAPI. Images shown are representative of n=48.

4.2 Accumulation in the Protoplasmic Cylinder

To determine the nature of the zones of HS-198 accumulation, *B. burgdorferi* spirochetes were co-stained with primary flagellin antibody (Figure 6). The flagellin antibody (red) rotates around HS-198 staining (blue). Since HS-198 must localize to an area within the flagellum rotation, this suggests that HS-198 accumulated inside the protoplasmic cylinder.

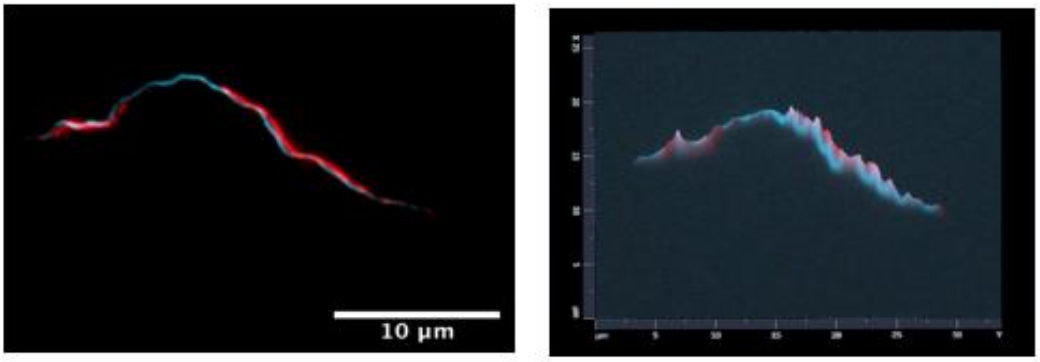

Figure 6: Confocal images (100x) of HS-198 (Blue) and Flagellin Ab. (Red) staining of a representative spirochete

Correlative Light Electron Microscopy (CLEM), a combination of fluorescent microscopy and high-resolution electron microscopy, confirmed separation from the outer membrane, and discrete spotting consistent with flagellum rotations blocking the signal, indicating localization of HS-198 inside the protoplasmic cylinder (Figure 7).

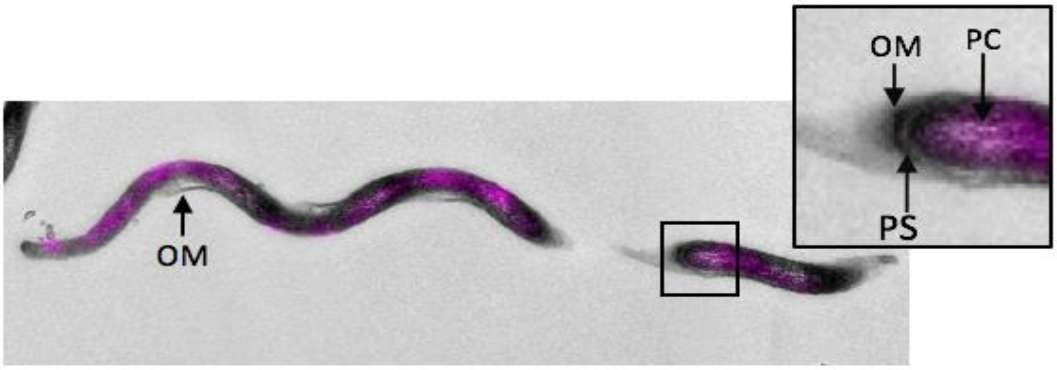

Figure 7: Correlative Light Electron Microscopy (CLEM) of HS-198 fluorescence overlaying a B. burgdorferi spirochete. Outer Membrane (OM), Protoplasmic Cylinder (PC) and Periplasmic Space (PS) are identified. Images shown are representative of n=4 spirochetes with TEM sections of 65 nm.

4.3 Accumulation in vivo

To test the feasibility of using HS-198 to detect *B. burgdorferi in vivo*, our collaborators in Dr. Monica Embers laboratory at the Tulane National Primate Research Center infected seven mice with approximately 500,000 spirochetes. After 3 weeks, HS-198 (25 nmol) was injected via the tail vein. Six hours post injection, the animals were euthanized and tissues from the ear, tibiotarsal joint, and spleen, areas where *B. burgdorferi* is known to localize in this model, were shipped to Duke for further sectioning. The sections were also co-stained with WGA and an anti-*B. burgdorferi* antibody. Examination of the sections by fluorescence microscopy identified *B. burgdorferi* in early and late stage aggregates in the ear and tibiotarsal joint (Figure 8A and B). Individual spirochetes were identified through HS-198 fluorescence as well as with anti-*B. burgdorferi* antibody (Figure 8C). Additionally, infected ear tissue from mice injected with HS-198 was co-stained with goat anti-rabbit conjugated with FITC as a non-specific antibody control to demonstrate the specificity of HS-198 *in vivo* (Figure 8D). These results demonstrate HS-198 selectivity for *B. burgdorferi* HtpG and localization to sites of *B. burgdorferi* infection in mice.

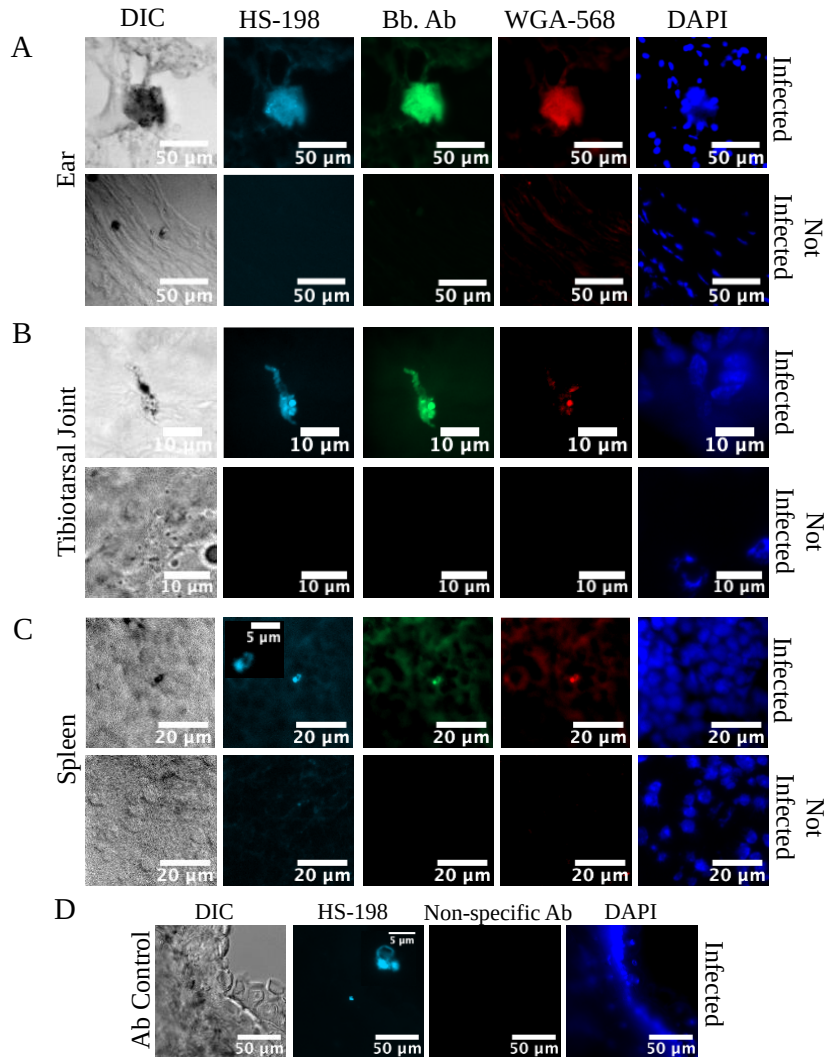

Figure 8: Fluorescence of tissues from mice infected with *B. burgdorferi* for 3 weeks and injected with HS-198 6 hours before sacrifice.(A) Ears (B) Tibiotarsal Joint and (C) Spleen were stained with FITC anti-*B. burgdorferi* antibody, WGA-568 (Extracellular Matrix), and DAPI (DNA). (D) Ears from mice injected with HS-198 were subsequently stained with goat anti-rabbit conjugated with FITC as a non-specific antibody consistent with the anti-borrelia antibody species. Images shown are representative of n=40 infected tissue samples and 15 uninfected.

In summary, we developed a fluorescent label which bound to HtpG to selectively identify the presence of Borrelia specific infection within mammalian tissues.

5. Discussion

This thesis describes an imaging agent able to exploit differences in the ATP binding site of a highly conserved, and highly expressed, heat shock protein, HtpG, to selectively target the stealth organism *B. burgdorferi* for a rapid diagnostic test of infection. HS-198 was previously developed as an inactive control molecule to demonstrate the selectivity of HS-131 for mammalian Hsp90 [64]. Fortuitously, when tested against purified recombinant *B. burgdorferi* HtpG, it was discovered the probe binds competitively to the proteins ATP binding site (Fig 4). The co-crystal structure of human Hsp90 with SNX2112 (an analog of the ligand portion of HS-131) shows an essential contact between D93 in the ATP binding site and the N2 nitrogen of the inhibitor [68]. The N,N-dimethylamide HS-198 analog disrupts the binding of the molecule to D93 of human Hsp90 [64]. The elution of *B. burgdorferi* GFP-HtpG with HS-198 may be due to distinct amino acid differences in the ATP binding pocket that can accommodate the N,N-dimethylamide. Testing HS-198 against recombinant forms of *E. coli* and *T. denticola* HtpGs lends support to this hypothesis. In particular, this molecule was inactive against *T. denticola* HtpG, reflecting that even small substitutions within the ATP binding site of related prokaryotic HtpG molecules is sufficient to alter the specificity for these small molecules. These results also suggest that HS-198 can be used to diagnose the presence of *B. burgdorferi in vivo* over the related oral spirochete. However, *E. coli* demonstrated similar binding to HS-198. Studies in cattle have identified the colon as the site for *E. coli* persistence and proliferation. As the colon is not

a common location of *B. burgdorferi* localization, clinical presentation and infection localization would likely allow for differentiation between infections of *B. burgdorferi* and *E. coli* [69]. However, future endeavors to modify the HS-198 ligand could improve species selectivity as well as increase the affinity.

HS-198 is able to accumulate inside living *B. burgdorferi* in detectable amounts in all life stages, and once internalized, confocal and CLEM imaging showed HS-198 co-localized around the flagella, suggesting accumulation inside of the protoplasmic cylinder (Fig 6). This accumulation inside of the spirochete points to an opportunity to utilize the HS-198 ligand as drug lead for a payload delivery of toxins or antibiotics. Linezolid, for example, has maintained antimicrobial activity when linked to a fluorescent probe [70]. Linezolid was also found to be in the top 20 most effective drugs against *B. burgdorferi* in a high throughput screen of new drug candidates. *B. burgdorferi* uptake of linezolid could possibly be improved by linkage to HS-198 ligand [71]. Finally, imaging of tissues from mice that were inoculated with HS-198 while alive found that HS-198 is able to disseminate, localize to, and identify active *B. burgdorferi* infection (Figure 8).

There is an unmet need for selective imaging agents that could non-invasively detect infection with sparse organisms that are difficult to locate and culture. Current methods primarily include cell culturing, histological examination, and serological assays. Culturing methods prove problematic as the hallmark of fastidious organisms is that they are difficult to culture. In the case of *B. burgdorferi*, culturing only yields a 3.1%

recovery rate from blood, or 45% recovery rate from erythema migrans rashes, which are only present in the initial stages of infection [72]. For detection using histological samples, invasive tissue biopsies are required, and there is a greater likelihood or scarce bacteria, such as *B. burgdorferi*, to be present but not in the location of the sample. Serological assays detect the presence of host antibodies to the bacteria. Cross- reactivity is a hurdle for diagnosis; for example patients with *B. quintana* infection may possess antibodies that are cross reactive with *Ch. Pneumonia*, *Chlamydia trachomatis*, and *Ch. psittac* [73]. Due to sequestration of antibody in antibody-antigen complexes and fluctuation in an antibody response, these tests become less inaccurate as the duration of infection increases which then often leads to false negative results, especially in the case of *B. burgdorferi* [74]. Targeting the host response for stealth organisms designed to evade the immune response is not an adequate means to assess the presence or absence of the organism. Methods to identify the etiology of the persistent symptoms in chronic Lyme Borreliosis are currently lacking as there are no non-invasive diagnostics available to determine whether there is an active infection or antibodies and remnants from a previous infection.

Direct detection of the pathogen confirms infection, and for this reason many researchers are turning to the development of imaging probes to visualize infection *in vivo*. Most imaging probes are targeting metabolic pathways which may be effective in actively replicating bacteria with high metabolic requirements but persister and stationary growth phase bacteria exhibit low metabolic activity and are therefore not

amenable to this approach [47].

To solve this problem, this work identified a protein that is expressed at high levels in all growth phases and morphological variants of *B. burgdorferi,* and, in order to identify persisting dormant bacteria, one that is not dependent upon active metabolism. Like its mammalian counterpart, Hsp90, HtpG is highly abundant at levels identifiable in the serum of infected patients, and by virtue of its ATP binding pocket, highly druggable. Although optical imaging probes tethered to HtpG have utility in histological and cellular studies, PET enabled versions of tethered selective small molecules may offer a non-invasive approach to detect unresolved *B. burgdorferi* infections by whole body imaging. This discovery that HS-198 is a *B. burgdorferi* selective probe that labels the bacteria both in culture and mice has broad implications for the development of a Lyme diagnostics or treatment.

Previous work with Hsp90 has led to verteporin-tethered Hsp90 inhibitors. Verteporfin is a photosensitizer for photodynamic therapy [75]. In addition, PET-labeled ligands for HSP90 have been studied for their use in the detection of cancer [76]. Future developments of HS-198 include a) agent detection using in vitro imaging systems (IVIS) that would allow imaging of a whole live mouse to identify active infection, b) modifications to the ligand to increase specificity and affinity, c) an exchange of the fluorescent molecule for a PET agent for imaging, and d) combining the HD-198 ligand with a toxin or antimicrobial agent to selectively deliver payloads to the bacteria for eradication. The goal is to eventually use these molecules in humans for the diagnosis

and eradication of disease.

6. Conclusions: Ongoing work and future directions

6.1 Imaging Live infection In Vivo

While Figure 8 effectively demonstrated the ability of HS-198 to localize to Borrelia on the microscopic level, it is necessary to determine if this probe could be used to identify infection within a whole, live animal. HS-198 is always fluorescent so optimal imaging requires time for the small molecule to clear from the non-infected sites and leave distinctive fluorescence which theoretically will correspond to the location of infection. To confirm that fact, luciferase expressing Borrelia is used so with an injection of luciferin, the precise location of the Borrelia within the mice may be imaged for an exact comparison to the fluorescence from HS-198.

In collaboration with Duke's Optical Molecular Imaging and Analysis core facility, 5 mice were anesthetized with 1-4% isoflurane and inoculated with approximately 500,000 luciferase expressing Borrelia spirochetes (strain JSB175) via subcutaneous injection the nape of the neck using a 25G needle. 4 mice were not infected. Drinking water for all mice contained 5 mg/ml streptomycin and 1 packet of Splenda/ 500 ml to mask the taste of the selection antibiotic for the luciferase vector. The luciferase expressing plasmid in the Borrelia contains a streptomycin resistant cassette, and the addition of streptomycin will continue bacterial selection *in vivo.* The mice were monitored for two weeks, at which time they were shaved and injected with 25 ul (12.5 nMol) of HS-198 into their right retro-orbital sinus. Following HS-198 injection, mice were imaged using in vitro imaging systems (IVIS) to identify active infection in whole

live mouse. Mice were imaged at 1, 3, 6, 9, and 24 hours post injection. 10 minutes prior to each imaging timepoint the mice would receive 150 mg/kg, via intraperitoneal injection, of luciferin. The mice were imaged for luminescence from the luciferase expressing borrelia, as well as fluorescence from HS-198.

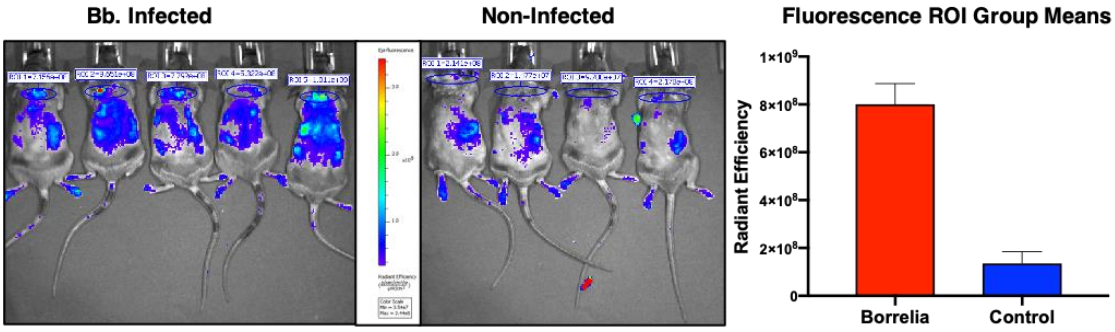

Figure 9: Fluorescent imaging and quantification of Borrelia infected (left) and non-infected (middle) mice 9 hours post HS-198 injection. The mean fluorescence from each group around the infection site at the neck, as circled, is quantified (right).

The fluorescence from HS-198 showed promising results, as seen hour 9 post HS-198 injection (Figure 9). The infected mice exhibited greater fluorescence overall but especially so at the site of infection (nape of the neck) as measured. Borrelia likely lingered at that location in the highest quantities as opposed to the low density dissemination throughout the rest of the body. We quantified the signal at every time point from the infection site corroborating the ability of HS-198 to differentiate infected vs non-infected mice (Figure 10). This was confirmed using a two two-way ANOVA with a repeated measure of time, and a two-stage linear step-up procedure of Benjamini, Krieger and Yekutieli method.

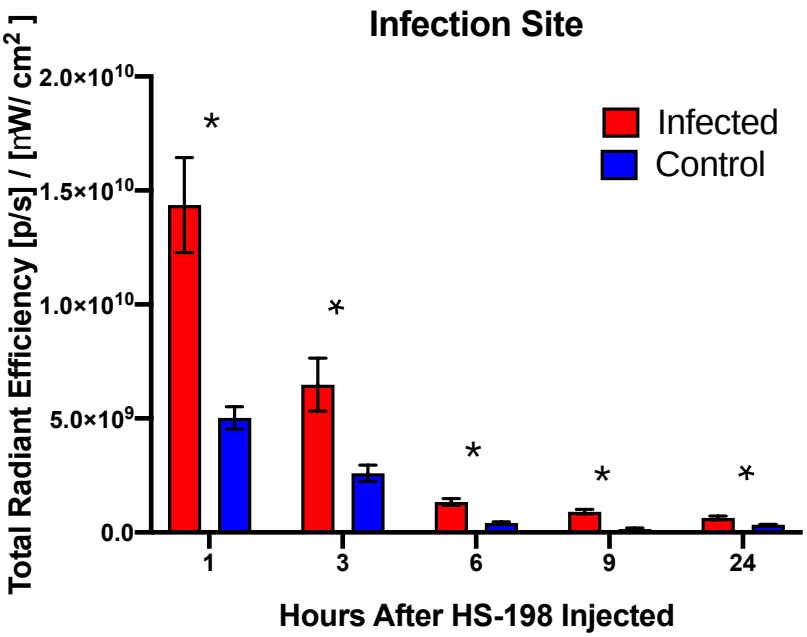

Figure 10: Quantification of the fluorescence at the site of infection and the snout of Borrelia infected and non-infected mice 1, 3, 6, 9, and 24 hours post HS-198 injection. Two-way ANOVA, repeated measure is time, two-stage linear step-up procedure of Benjamini, Krieger and Yekutieli method, * = $p < 0.05$.

Unfortunately, only 2 of the 5 infected mice had significant luminescent signal post luciferin injected. Possibilities for this could be loss of the plasmid associated with luciferase expression in the Borrelia. Otherwise, the mice could have cleared the infection and the increase of HS-198 signal was due to binding of the remnant Borrelia proteins. The luciferase expression from one of the mice that did produce a luminescent signal is compared to the HS-198 signal at the same time point (Figure 11). The signal especially at the sight of infection offers a promising indication that HS-198 is localizing to and fluorescing from the site of Borrelia infection as seen in Figure 11.

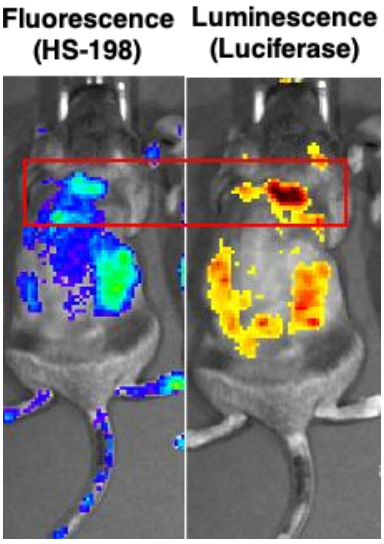

Figure 11: Fluorescence vs Luminescence of a Borrelia infected mouse 8 hours post HS-198 injection. Fluorescence (left) is from HS-198, luminescence (right) is from the luciferase expressing Borrelia.

Follow up experiments have included an arm of infected mice treated 1 week after infection with 16 mg/kg of ceftriaxone diluted in PBS, twice a day for 5 days. qPCR was performed on heart, skin from the injection site, bladder, left pinna, left tibiotarsal joint, and the nose. All ten of the infected mice from that experiment were PCR positive (data not shown) for Borrelia in the tissues, and all ten of the ceftriaxone treated animals were PCR negative for Borrelia. Follow up imaging experiments will include this treated group to determine if Borrelia remnants from past infection are distinguishable from active infection. As mentioned, future work hopes to improve HS-198 binding in order to be able to measure low density infections with higher accuracy. Furthermore, future studies hope to use radiolabeled ligands that would allow imaging at increased tissue depths for a more complete view.

6.2 The Search for Improved Lead Ligands

While HS-198 is an intriguing ligand, an ideal ligand with greater inhibitory activity and affinity while maintaining selectivity would be preferable. We sought to find a lead ligand that would be more potent with as much, if not greater, species selectivity. In a small FLECS screen of inhibitors identified by homologues structure, we identified HSX-2450 as a possible lead for future optimization. Results are displayed as fold change of signal from GFP-tagged elutions. While HSX-2450 is most effective in binding E. coli, the affinity for Borrelia is double that of HS-198, and still ineffective against mammalian Hsp90. Future work will seek to optimize this ligand to preferentially bind Borrelia, however, this ligand could also be used as it is for work with *E. coli*. HSX-3876 was not as promising for Borrelia however showed incredible activity for *T. denticola* and could be a lead ligand for research against the oral spirochete.

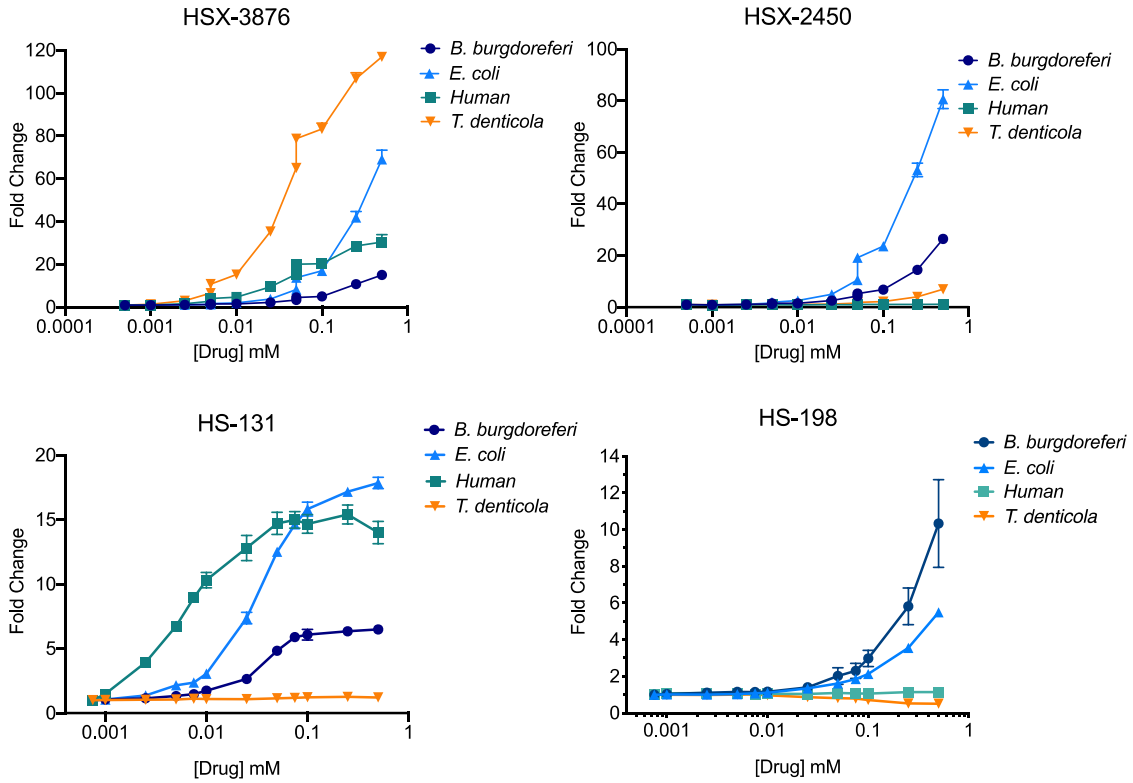

Figure 12:Elutions of Analogue structures to find more potent inhibitor. Fluorescent signal quantified from FLECS assay of GFP-tagged HTPG homologues (n=3).

6.3 Identifying the Binding Domain

D93 of mammalian Hsp90 has been identified as a critical binding site in the ATP binding region. [77] [59]. As this Aspartic Acid is conserved in the ATP binding domain of all analyzed species (Figure 2), we investigated whether the amino acids flanking this conserved AA would increase the variability in drug binding seen in Figure 3 and 4. GFP tagged full length recombinant proteins of Hsp90 and HtpG incorporating the point mutations described in Table 3 were created.

Table 3: Point mutation location

Location	Wild Type	Mutation
Human Hsp90 (AA 92-94)	V-D-T	K-D-N
Borrelia HtpG (AA 73-75)	K-D-N	V-D-T

A FLECS assay as described previously was performed on the recombinant proteins and the proteins were eluted from the column with HS-198, HS-10, HSX-2450, and Ganetespib. The signal quantified from eluted proteins is displayed in Figure 13, mutations are notated by **.

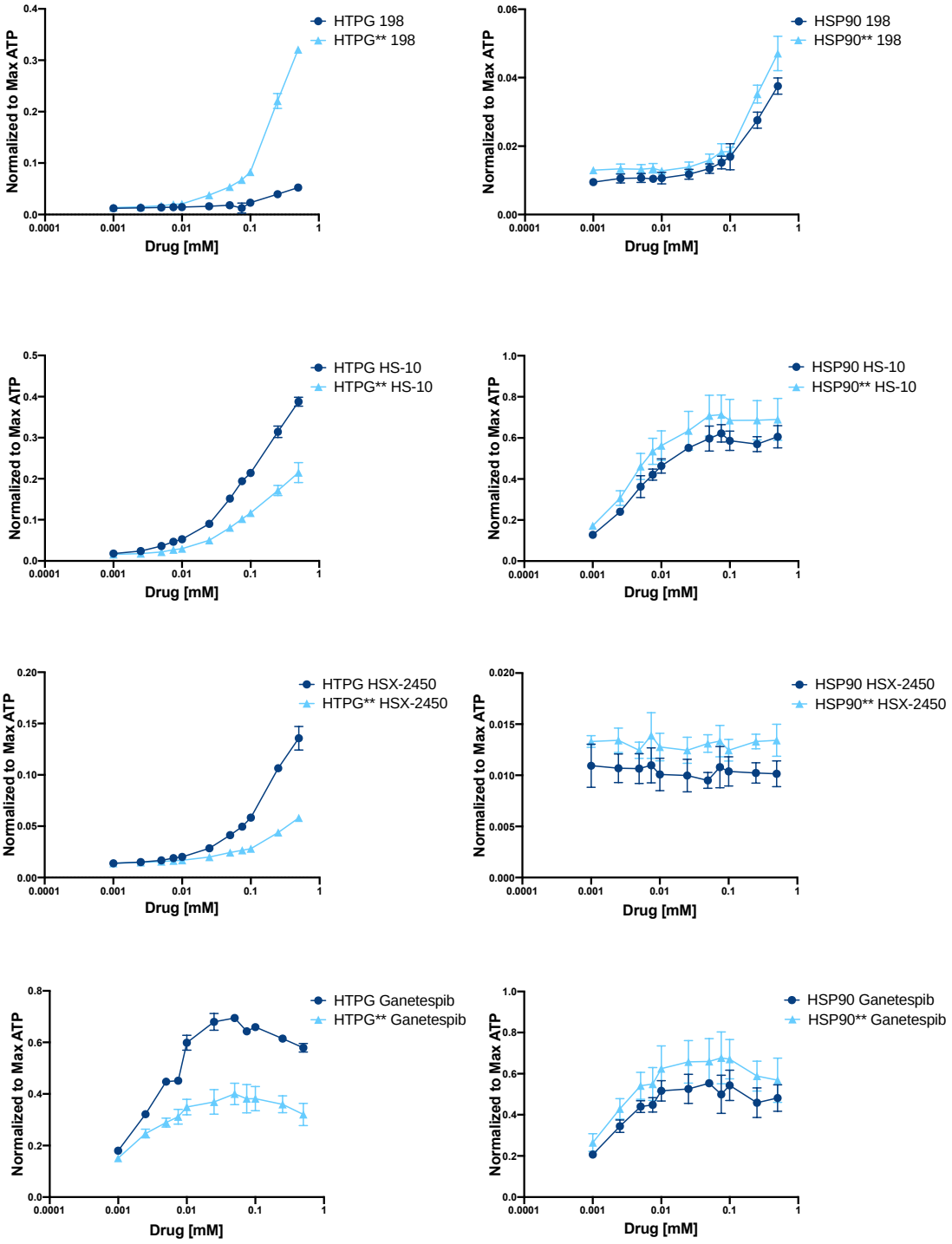

Figure 13: Elution profiles of GFP tagged- point mutated Hsp90 and HtpG. Mutations as described in Table 3 and marked with **. Performed in technical and biological duplicate.

This experiment was performed in technical duplicate and then replicated producing consistent results. The point mutations of HSP90 had an insignificant effect. The mutations of HtpG diminished the binding capacity of all inhibitors except one. HtpG mutations created a notable increase in binding capacity to HS-198. The implications of this result require further investigation but points to a need to investigate each binding site carefully by developing a crystal structure of the HS-198 ligand bound to Borrelia HtpG. A crystal structure will identify other specific locations that can be adapted on the small molecule ligand to further differentiate its binding capabilities across species.

ATP binding takes place in the N-terminal of the ATP binding domain. Previous work has investigated the confirmational changes associated with ATP binding in mammalian and yeast Hsp90 and concluded they are localized to the N-terminal domain [78, 79]. While the C-terminal might not be directly associated with this binding, we wanted to investigate whether the differences associated with the C-terminal could hinder or improve access for these inhibitors to the binding site.

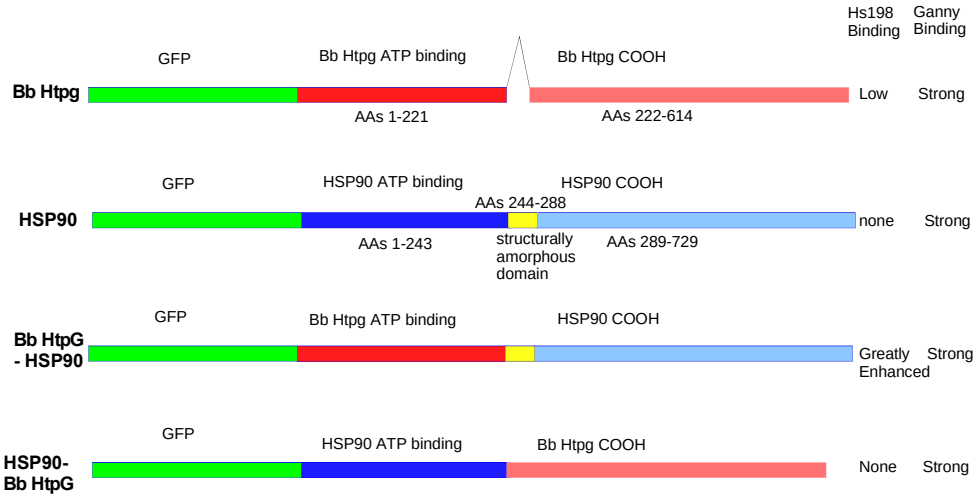

Figure 14: Borrelia HtpG and mammalian ATP domain swap (Dr. Alcorta). Sample design for Figure 15 of full length Borrelia HtpG, mammalian Hsp90, and mutants of swapped N- and C- terminals.

Full length Borrelia HtpG, mammalian Hsp90, and mutants swapping the N- and C-terminals were created. A FLECS assay was performed as previously described and the proteins were eluted with HS-198 or Ganetespib. Results are seen in Figure 15.

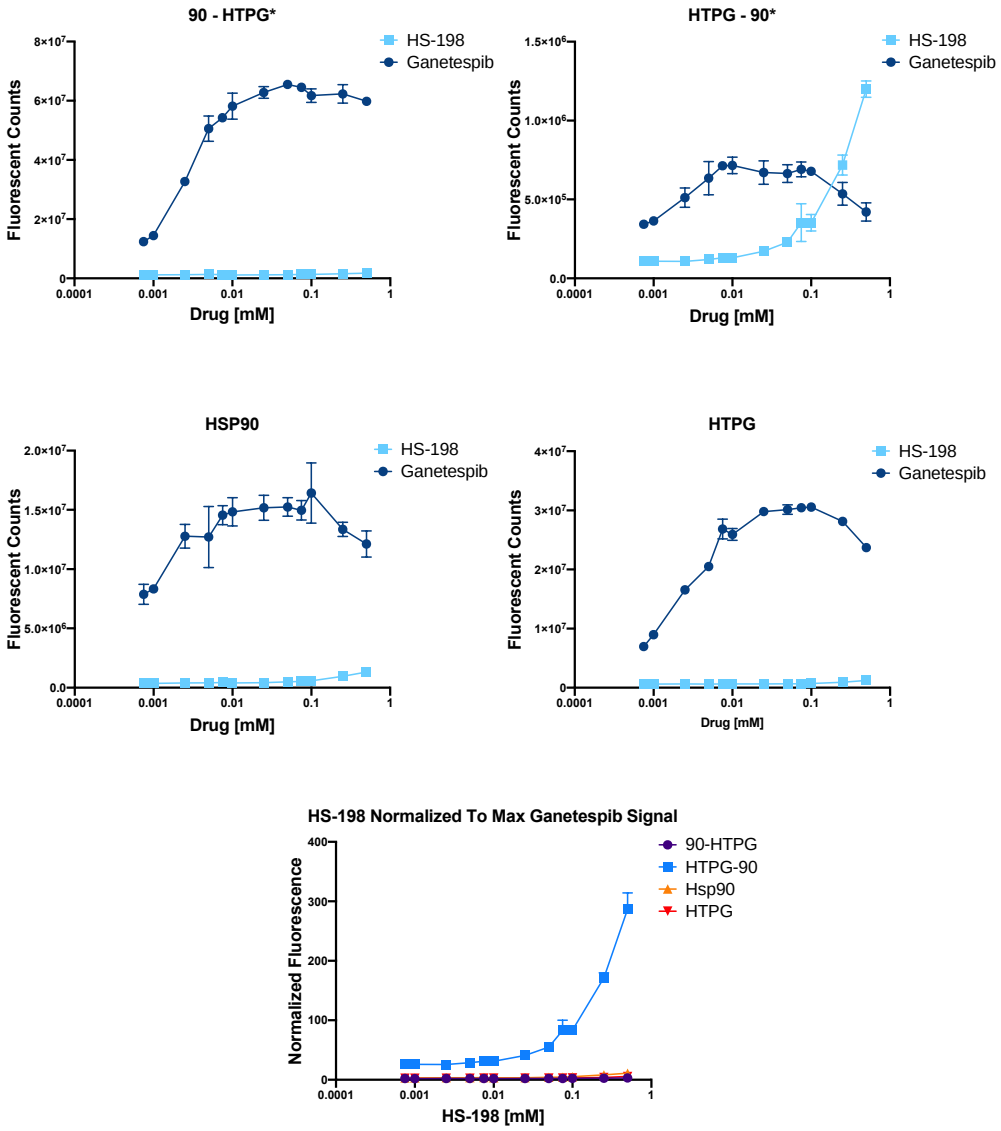

Figure 15: Effect of Domain swap of N and C terminals of mammalian Hsp90 and Borrelia HtpG on HS-198 and Ganetespib binding. Mutant indicated by *. Performed in technical and biological duplicate.

Swapping the C-terminal of Hsp90 with the C-terminal of HtpG resulted in no significant difference in binding. Swapping the C-terminal of HtpG however resulted in a significant increase of HS-198 binding. HS-198 was normalized to the Ganetespib, which has previously demonstrated the most consistent, non-species specific binding (Figure 3), to confirm the increase in binding capacity in this mutant. The HtpG mutant

contained the amorphous domain that is only present in the WT Hsp90 (portrayed as yellow in Figure 14) and we hypothesize that this region could impact the structure configuration of the protein possibly increasing access to the binding site. Future work will compare the mutant with and without this amorphous region to confirm.

6.4 Heat Shock Experiment

In alternative medicine, induced hyperthermia has been a common treatment for patients with Lyme disease. While there is a great deal of anecdotal evidence that points to the efficacy of this treatment, there has yet to be a thorough scientific investigation into these claims. In Borrelia, stationary phase and persister bacteria are the focus for new treatments as logarithmic phase are easily eradicated with common antibiotics. This is one of many reasons that delayed treatment leads to increased comorbidities. Reiterating what is already known, we have found a lack of substantial phenotypic response to HtpG inhibition of stationary phase Borrelia at the standard 34 °C. Additionally, we found negligible effects of Doxorubicin, a chemotherapy treatment that prior literature determines should be effective in killing Borrelia [71]. Rather than seek out new drug targets, we sought to determine if higher temperatures (40°C) would increase the efficacy of these treatments.

We developed a protocol to measure the efficacy of these drugs alone and in combination. Borrelia were grown to stationary phase (~8 days, $10^7 - 10^8$cells/mL) and then plated in 96 well plates in combination with a matrix of Doxorubicin and Ganetespib. The treatments were diluted in DMSO, and total DMSO per well was

equalized. The plates were sealed containing only a small amount of air as Borrelia are microaerophilic and will not thrive in the presence of atmospheric levels of oxygen. The plates were then placed in either 34°C or 40 °C incubators. Daily, one plate was removed from each temperature and a viability assay performed. Plates were centrifuged to adhere the Borrelia to the bottom, and the media removed. The Borrelia were eluted in 50 µl of PBS and 50 µl of Bactiter Glo (WT). The signal was quantified by a Spectramax iD5 microplate reader (Figure 16). This experiment is preliminary, the culture at 40 °C was performed at a different time as 34 °C, but Borrelia cultures were grown to the same starting density. The Ganetespib dilution was slightly different, as seen on the X-axis. Comparison is being made for discussion of future directions only.

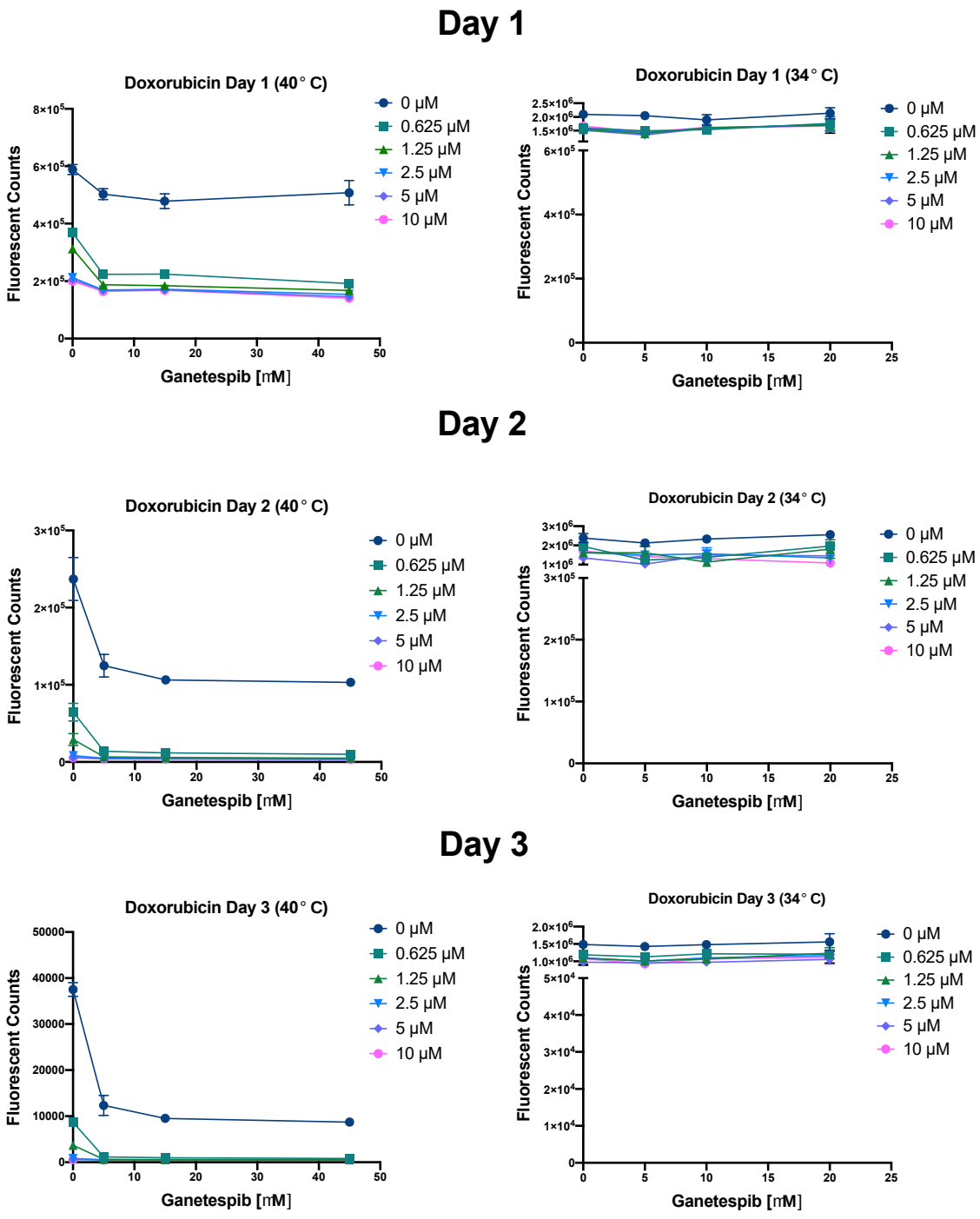

Figure 16: Day 1, 2, and 3 of Heat Shock Experiment. Viability assay of stationary phase Borrelia combined with a matrix of Doxorubicin and Ganetespib (n=2).

Statistical analysis of the effect of Ganetespib and Doxorubicin is seen in Figure 17. The number of Borrelia in the wells treated only with DMSO (0 μM of both drugs) decreased each day at 40 °C but stayed consistent at 34 °C. Furthermore, the drug effect was negligible at 34 °C.

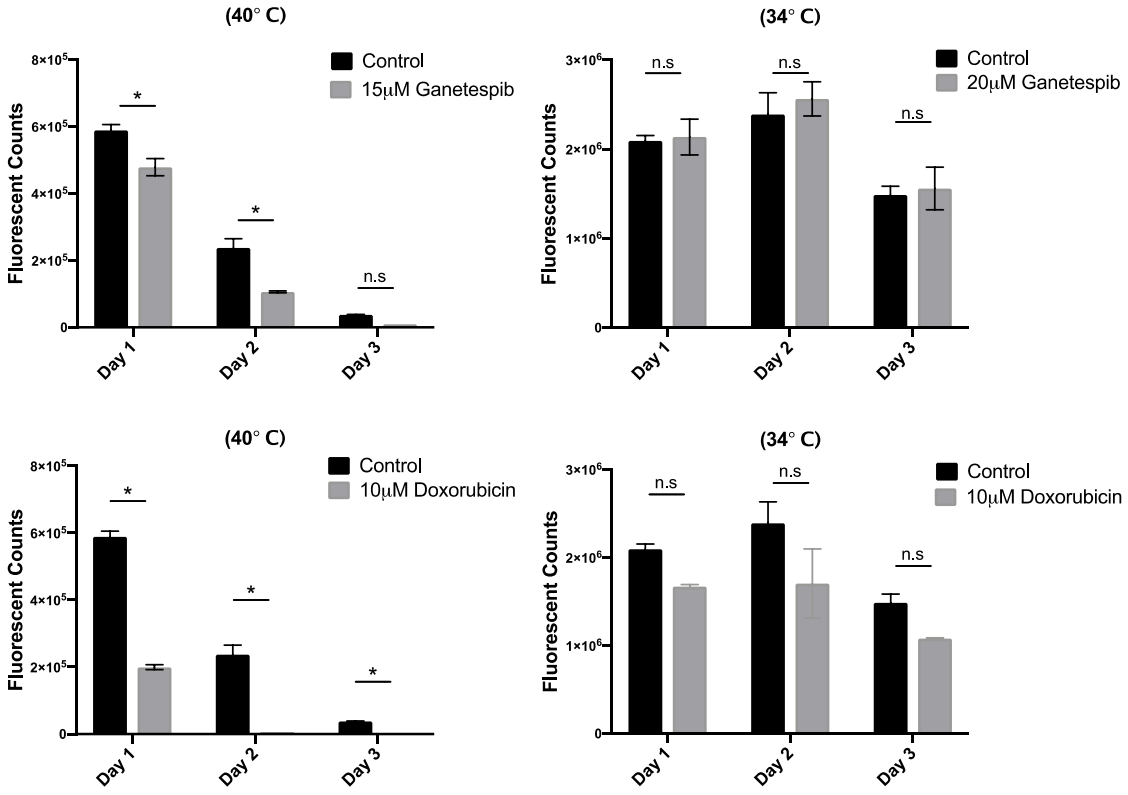

Figure 17: Statistical analysis of Heat Shock Experiment. Multiple t Test, *=P< .01

20 μM of Ganetespib had statistically insignificant effects at 34 °C but 15 μM had significant effects at 40 °C. 10 μM of Doxorubicin has statistically significant effect at 40 °C but not at 34 °C. These results reveal that the heat increases the death of Borrelia independent of drug and moreover increases the efficacy of Doxorubicin and Ganetespib (Figure 17). Furthermore, Ganetespib and Doxorubicin in combination was

an effective treatment. Future work will explore if this effect is synergistic or additive. This experiment was performed once again substituting Doxorubicin for Disulfiram, a drug used for the treatment of alcoholism that has been identified as effective against Borrelia, but once again was not effective against stationary phase Borrelia at standard temperatures in our lab [71]. Results were consistent with Doxorubicin.

The inhibitors investigated, disulfiram and doxorubicin, are highly toxin treatments. If hyperthermic conditions could decrease the required dose to achieve the therapeutic window, adverse side effects could hopefully be avoided. In addition, this work opens up the possibilities of utilizing a Borrelia specific potent HtpG inhibitor in combination with hyperthermia or with hyperthermia and other treatments. This pilot study launches a new wave of possibilities for the treatment of patients.

In summation, these initial studies validate the opportunity to create more potent and selective ligands. Once improved these molecules could advance to use in humans to act as payload deliveries for imaging agents or anti-microbials. In addition, the heat shock studies suggest a very exciting direction for patient treatment. Hyperthermia is already commonly used as an alternative therapy for Lyme, and these results preliminarily validate this method. With further research this method could become a more commonly applied treatment for patients. In addition, treating patients with a heat shock protein inhibitor is a new method that deserves further exploration for patient treatment. Lyme disease is a devastating disease for many people, and unfortunately there are no clear treatment plan for patients with chronic symptoms, and possibly

chronic infection. This study highlights a number of encouraging directions that could revolutionize treatment possibilities for these patients.

References

1. Mead, P.S., *Epidemiology of Lyme disease.* Infect Dis Clin North Am, 2015. **29**(2): p. 187-210.

2. Nelson, C.A., et al., *Incidence of Clinician-Diagnosed Lyme Disease, United States, 2005-2010.* Emerg Infect Dis, 2015. **21**(9): p. 1625-31.

3. Kugeler, K.J., et al., *Geographic Distribution and Expansion of Human Lyme Disease, United States.* Emerg Infect Dis, 2015. **21**(8): p. 1455-7.

4. Eisen, R.J., L. Eisen, and C.B. Beard, *County-Scale Distribution of Ixodes scapularis and Ixodes pacificus (Acari: Ixodidae) in the Continental United States.* J Med Entomol, 2016. **53**(2): p. 349-86.

5. Auwaerter, P.G., J. Aucott, and J.S. Dumler, *Lyme borreliosis (Lyme disease): molecular and cellular pathobiology and prospects for prevention, diagnosis and treatment.* Expert Rev Mol Med, 2004. **6**(2): p. 1-22.

6. Ogden, N.H., et al., *Investigation of relationships between temperature and developmental rates of tick Ixodes scapularis (Acari: Ixodidae) in the laboratory and field.* J Med Entomol, 2004. **41**(4): p. 622-33.

7. Dumic, I. and E. Severnini, *"Ticking Bomb": The Impact of Climate Change on the Incidence of Lyme Disease.* Can J Infect Dis Med Microbiol, 2018. **2018**: p. 5719081.

8. Li, S., et al., *Consequences of landscape fragmentation on Lyme disease risk: a cellular automata approach.* PLoS One, 2012. **7**(6): p. e39612.

9. Cook, M.J., *Lyme borreliosis: a review of data on transmission time after tick attachment.* Int J Gen Med, 2015. **8**: p. 1-8.

10. des Vignes, F., et al., *Effect of tick removal on transmission of Borrelia burgdorferi and Ehrlichia phagocytophila by Ixodes scapularis nymphs.* J Infect Dis, 2001. **183**(5): p. 773-8.

11. Wikel, S., *Ticks and tick-borne pathogens at the cutaneous interface: host defenses, tick countermeasures, and a suitable environment for pathogen establishment.* Front Microbiol, 2013. **4**: p. 337.

12. Vachiery, N., et al., *An in vitro model to assess the immunosuppressive effect of tick saliva on the mobilization of inflammatory monocyte-derived cells.* Vet Res, 2015. **46**: p. 117.
13. Wormser, G.P., et al., *The clinical assessment, treatment, and prevention of lyme disease, human granulocytic anaplasmosis, and babesiosis: clinical practice guidelines by the Infectious Diseases Society of America.* Clin Infect Dis, 2006. **43**(9): p. 1089-134.
14. Vig, D.K. and C.W. Wolgemuth, *Spatiotemporal evolution of erythema migrans, the hallmark rash of Lyme disease.* Biophys J, 2014. **106**(3): p. 763-8.
15. DePietropaolo, D.L., et al., *Diagnosis of lyme disease.* Am Fam Physician, 2005. **72**(2): p. 297-304.
16. Hildenbrand, P., et al., *Lyme neuroborreliosis: manifestations of a rapidly emerging zoonosis.* AJNR Am J Neuroradiol, 2009. **30**(6): p. 1079-87.
17. Scieszka, J., J. Dabek, and P. Cieslik, *Post-Lyme disease syndrome.* Reumatologia, 2015. **53**(1): p. 46-8.
18. Kwit, N.A., et al., *Risk Factors for Clinician-Diagnosed Lyme Arthritis, Facial Palsy, Carditis, and Meningitis in Patients From High-Incidence States.* Open Forum Infect Dis, 2018. **5**(1): p. ofx254.
19. Miklossy, J., *Alzheimer's disease - a neurospirochetosis. Analysis of the evidence following Koch's and Hill's criteria.* J Neuroinflammation, 2011. **8**: p. 90.
20. Kenedy, M.R., T.R. Lenhart, and D.R. Akins, *The role of Borrelia burgdorferi outer surface proteins.* FEMS Immunol Med Microbiol, 2012. **66**(1): p. 1-19.
21. Nigrovic, L.E. and K.M. Thompson, *The Lyme vaccine: a cautionary tale.* Epidemiol Infect, 2007. **135**(1): p. 1-8.
22. Poland, G.A., *Vaccines against Lyme disease: What happened and what lessons can we learn?* Clin Infect Dis, 2011. **52 Suppl 3**: p. s253-8.
23. Comstedt, P., et al., *The novel Lyme borreliosis vaccine VLA15 shows broad protection against Borrelia species expressing six different OspA serotypes.* PLoS One, 2017. **12**(9): p. e0184357.
24. Vogt, N.A., et al., *Efficacy of Borrelia burgdorferi vaccine in dogs in North America: A systematic review and meta-analysis.* J Vet Intern Med, 2019. **33**(1): p. 23-36.

25. Hirsch, A.G., et al., *Obstacles to diagnosis and treatment of Lyme disease in the USA: a qualitative study.* BMJ Open, 2018. **8**(6): p. e021367.

26. Di Domenico, E.G., et al., *The Emerging Role of Microbial Biofilm in Lyme Neuroborreliosis.* Front Neurol, 2018. **9**: p. 1048.

27. Donlan, R.M., *Biofilms: microbial life on surfaces.* Emerg Infect Dis, 2002. **8**(9): p. 881-90.

28. Merilainen, L., et al., *Morphological and biochemical features of Borrelia burgdorferi pleomorphic forms.* Microbiology (Reading), 2015. **161**(Pt 3): p. 516-27.

29. Sapi, E., et al., *Evidence of In Vivo Existence of Borrelia Biofilm in Borrelial Lymphocytomas.* Eur J Microbiol Immunol (Bp), 2016. **6**(1): p. 9-24.

30. Hochstim, C.J., R. Masood, and D.H. Rice, *Biofilm and persistent inflammation in endoscopic sinus surgery.* Otolaryngol Head Neck Surg, 2010. **143**(5): p. 697-8.

31. Hoiby, N., et al., *Antibiotic resistance of bacterial biofilms.* Int J Antimicrob Agents, 2010. **35**(4): p. 322-32.

32. Tankersley, A., et al., *Early effects of Staphylococcus aureus biofilm secreted products on inflammatory responses of human epithelial keratinocytes.* J Inflamm (Lond), 2014. **11**: p. 17.

33. Anderl, J.N., et al., *Role of nutrient limitation and stationary-phase existence in Klebsiella pneumoniae biofilm resistance to ampicillin and ciprofloxacin.* Antimicrob Agents Chemother, 2003. **47**(4): p. 1251-6.

34. Rudenko, N., et al., *Isolation of live Borrelia burgdorferi sensu lato spirochaetes from patients with undefined disorders and symptoms not typical for Lyme borreliosis.* Clin Microbiol Infect, 2016. **22**(3): p. 267 e9-15.

35. Embers, M.E., et al., *Persistence of Borrelia burgdorferi in rhesus macaques following antibiotic treatment of disseminated infection.* PLoS One, 2012. **7**(1): p. e29914.

36. Crossland, N.A., X. Alvarez, and M.E. Embers, *Late Disseminated Lyme Disease: Associated Pathology and Spirochete Persistence Posttreatment in Rhesus Macaques.* Am J Pathol, 2018. **188**(3): p. 672-682.

37. Hodzic, E., et al., *Persistence of Borrelia burgdorferi following antibiotic treatment in mice.* Antimicrob Agents Chemother, 2008. **52**(5): p. 1728-36.

38. Aucott, J.N., et al., *Post-treatment Lyme disease syndrome symptomatology and the impact on life functioning: is there something here?* Qual Life Res, 2013. **22**(1): p. 75-84.

39. Doern, G.V., *Detection of selected fastidious bacteria.* Clin Infect Dis, 2000. **30**(1): p. 166-73.

40. Prevention, C.f.D.C.a. *Two-tiered Testing Decision Tree*. CDC.gov 2011.

41. Cook, M.J. and B.K. Puri, *Commercial test kits for detection of Lyme borreliosis: a meta-analysis of test accuracy.* Int J Gen Med, 2016. **9**: p. 427-440.

42. Dattwyler, R.J., et al., *Seronegative Lyme disease. Dissociation of specific T- and B-lymphocyte responses to Borrelia burgdorferi.* N Engl J Med, 1988. **319**(22): p. 1441-6.

43. Haupl, T., et al., *Persistence of Borrelia burgdorferi in ligamentous tissue from a patient with chronic Lyme borreliosis.* Arthritis Rheum, 1993. **36**(11): p. 1621-6.

44. Weinstein, E.A., et al., *Imaging Enterobacteriaceae infection in vivo with 18F-fluorodeoxysorbitol positron emission tomography.* Sci Transl Med, 2014. **6**(259): p. 259ra146.

45. Gowrishankar, G., et al., *Specific Imaging of Bacterial Infection Using 6''-(18)F-Fluoromaltotriose: A Second-Generation PET Tracer Targeting the Maltodextrin Transporter in Bacteria.* J Nucl Med, 2017. **58**(10): p. 1679-1684.

46. Rahman, W.T., et al., *The impact of infection and inflammation in oncologic (18)F-FDG PET/CT imaging.* Biomed Pharmacother, 2019. **117**: p. 109168.

47. Rudenko, N., et al., *Metamorphoses of Lyme disease spirochetes: phenomenon of Borrelia persisters.* Parasit Vectors, 2019. **12**(1): p. 237.

48. Norris, S.J., *Antigenic variation with a twist--the Borrelia story.* Mol Microbiol, 2006. **60**(6): p. 1319-22.

49. Schopf, F.H., M.M. Biebl, and J. Buchner, *The HSP90 chaperone machinery.* Nat Rev Mol Cell Biol, 2017. **18**(6): p. 345-360.

50. Lopez, J.E., et al., *Identification of conserved antigens for early serodiagnosis of relapsing fever Borrelia.* Microbiology (Reading), 2009. **155**(Pt 8): p. 2641-2651.

51. Taipale, M., D.F. Jarosz, and S. Lindquist, *HSP90 at the hub of protein homeostasis: emerging mechanistic insights.* Nat Rev Mol Cell Biol, 2010. **11**(7): p. 515-28.

52. Rodriguez, I., et al., *Prevalence of antibodies to Borrelia burgdorferi sensu stricto in humans from a Cuban village.* Braz J Infect Dis, 2012. **16**(1): p. 82-5.

53. Grudniak, A.M., B. Klecha, and K.I. Wolska, *Effects of null mutation of the heat-shock gene htpG on the production of virulence factors by Pseudomonas aeruginosa.* Future Microbiol, 2018. **13**: p. 69-80.

54. Verbrugghe, E., et al., *HtpG contributes to Salmonella Typhimurium intestinal persistence in pigs.* Vet Res, 2015. **46**: p. 118.

55. Shelburne, C.E., et al., *HtpG, the Porphyromonas gingivalis HSP-90 homologue, induces the chemokine CXCL8 in human monocytic and microvascular vein endothelial cells.* Cell Microbiol, 2007. **9**(6): p. 1611-9.

56. Yamanaka, T., et al., *Gene expression profile and pathogenicity of biofilm-forming Prevotella intermedia strain 17.* BMC Microbiol, 2009. **9**: p. 11.

57. Whitesell, L., et al., *Structural basis for species-selective targeting of Hsp90 in a pathogenic fungus.* Nat Commun, 2019. **10**(1): p. 402.

58. Batista, F.A.H., et al., *Discovery of small molecule inhibitors of Leishmania braziliensis Hsp90 chaperone.* J Enzyme Inhib Med Chem, 2020. **35**(1): p. 639-649.

59. Posfai, D., et al., *Identification of Hsp90 Inhibitors with Anti-Plasmodium Activity.* Antimicrob Agents Chemother, 2018. **62**(4).

60. Nakamoto, H., et al., *Physical interaction between bacterial heat shock protein (Hsp) 90 and Hsp70 chaperones mediates their cooperative action to refold denatured proteins.* J Biol Chem, 2014. **289**(9): p. 6110-9.

61. Haystead, T.A.J., *Fluorescent-Linked Enzyme Chemoproteomic Strategy (FLECS) for Identifying HSP70 Inhibitors.* Methods Mol Biol, 2018. **1709**: p. 75-86.

62. Haystead, C.M., et al., *Gamma-phosphate-linked ATP-sepharose for the affinity purification of protein kinases. Rapid purification to homogeneity of skeletal muscle mitogen-activated protein kinase kinase.* Eur J Biochem, 1993. **214**(2): p. 459-67.

63. Jhaveri, K., et al., *Heat shock protein 90 inhibitors in the treatment of cancer: current status and future directions.* Expert Opin Investig Drugs, 2014. **23**(5): p. 611-28.

64. Crowe, L.B., et al., *A Fluorescent Hsp90 Probe Demonstrates the Unique Association between Extracellular Hsp90 and Malignancy in Vivo.* ACS Chem Biol, 2017. **12**(4): p. 1047-1055.

65. Richter, K., et al., *Conserved conformational changes in the ATPase cycle of human Hsp90.* J Biol Chem, 2008. **283**(26): p. 17757-65.

66. Graf, C., et al., *Spatially and kinetically resolved changes in the conformational dynamics of the Hsp90 chaperone machine.* EMBO J, 2009. **28**(5): p. 602-13.

67. Shimamura, T., et al., *Ganetespib (STA-9090), a nongeldanamycin HSP90 inhibitor, has potent antitumor activity in in vitro and in vivo models of non-small cell lung cancer.* Clin Cancer Res, 2012. **18**(18): p. 4973-85.

68. Fadden, P., et al., *Application of chemoproteomics to drug discovery: identification of a clinical candidate targeting hsp90.* Chem Biol, 2010. **17**(7): p. 686-94.

69. Grauke, L.J., et al., *Gastrointestinal tract location of Escherichia coli O157:H7 in ruminants.* Appl Environ Microbiol, 2002. **68**(5): p. 2269-77.

70. Phetsang, W., et al., *An azido-oxazolidinone antibiotic for live bacterial cell imaging and generation of antibiotic variants.* Bioorg Med Chem, 2014. **22**(16): p. 4490-8.

71. Pothineni, V.R., et al., *Identification of new drug candidates against Borrelia burgdorferi using high-throughput screening.* Drug Des Devel Ther, 2016. **10**: p. 1307-22.

72. Doern, G.V., *Detection of selected fastidious bacteria.* Clinical Infectious Diseases, 2000. **30**(1): p. 166-173.

73. Brouqui, P. and D. Raoult, *New insight into the diagnosis of fastidious bacterial endocarditis.* FEMS Immunol Med Microbiol, 2006. **47**(1): p. 1-13.

74. Schutzer, S.E., et al., *Borrelia burgdorferi-specific immune complexes in acute Lyme disease.* JAMA, 1999. **282**(20): p. 1942-6.

75. Kaneko, K., et al., *Heat shock protein 90-targeted photodynamic therapy enables treatment of subcutaneous and visceral tumors.* Commun Biol, 2020. **3**(1): p. 226.

76. Wang, X., et al., *PET imaging of Hsp90 expression in pancreatic cancer using a new (64)Cu-labeled dimeric Sansalvamide A decapeptide.* Amino Acids, 2018. **50**(7): p. 897-907.

77. Bozdech, Z., et al., *The transcriptome of the intraerythrocytic developmental cycle of Plasmodium falciparum.* PLoS Biol, 2003. **1**(1): p. E5.

78. Karagoz, G.E., et al., *N-terminal domain of human Hsp90 triggers binding to the cochaperone p23.* Proc Natl Acad Sci U S A, 2011. **108**(2): p. 580-5.

79. Giannoulis, A., et al., *Two closed ATP- and ADP-dependent conformations in yeast Hsp90 chaperone detected by Mn(II) EPR spectroscopic techniques.* Proc Natl Acad Sci U S A, 2020. **117**(1): p. 395-404.

Biography

While at Duke University, Madeline Sell spent three years on Duke's Institutional Review Board (IRB) as a voting member to ensure ethical and responsible research conduct within Duke's scientific studies. She passed the patent bar to become a patent agent for the US Patent and Trademark Office. Additionally, she was the representative for the Dept of Pharmacology on the Graduate and Professional Student Council (GPSC) for three years. She was a fellow in the Tech Transfer Fellows Program in Duke's Office of licensing and Ventures assessing the commercial viability of innovative Duke technologies.

Prior to graduate school she attended Tulane University after receiving a merit based presidential scholarship. She worked with Tulane's Dept of Mathematics to utilize pressurized capillary tubes to demonstrate unidirectional flow of sea urchin sperm in order to help create a mathematical model of sperm flagellum motion. In addition, she worked in a lab of Tulane's Dept of Chemical Engineering to help measure the flow patterns of surfactants in combination with crude oil from the BP oil spill. While at Tulane she also worked at the Louisiana Cancer Research Center and received a donor grant to research the effects of cadmium and nickel exposure. She graduated from Tulane University with a BSE in Chemical and Biomolecular Engineering.